Cell. Mol. Life Sci. (2012) 69:129–148
DOI 10.1007/s00018-011-0739-x

Cellular and Molecular Life Sciences

RESEARCH ARTICLE

An abundant, truncated human sulfonylurea receptor 1 splice variant has prodiabetic properties and impairs sulfonylurea action

Diethart Schmid · Michael Stolzlechner · Albin Sorgner · Caterina Bentele · Alice Assinger · Peter Chiba · Thomas Moeslinger

Received: 2 December 2010 / Revised: 20 May 2011 / Accepted: 23 May 2011 / Published online: 14 June 2011

Abstract An alternatively spliced form of human sulfonylurea receptor (SUR) 1 mRNA lacking exon 2 (SUR1Δ2) has been identified. The omission of exon 2 caused a frame shift and an immediate stop codon in exon 3 leading to translation of a 5.6-kDa peptide that comprises the N-terminal extracellular domain and the first transmembrane helix of SUR1. Based on a weak first splice acceptor site in the human SUR1 gene (ABCC8), RT-PCR revealed a concurrent expression of SUR1Δ2 and SUR1. The SUR1Δ2/(SUR1 + SUR1Δ2) mRNA ratio differed between tissues, and was lowest in pancreas (46%), highest in heart (88%) and negatively correlated with alternative splice factor/splicing factor 2 (ASF/SF2) expression. In COS-7 cells triple transfected with SUR1Δ2/SUR1/Kir6.2, the SUR1Δ2 peptide co-immunoprecipitated with Kir6.2, thereby displacing two of four SUR1 subunits on the cell surface. The ATP sensitivity of these hybrid ATP-sensitive potassium channels (K_{ATP}) channels was reduced by about sixfold, as shown with single-channel recordings. RINm5f rat insulinoma cells, which genuinely express SUR1 but not SUR1Δ2, exhibited a strongly increased K_{ATP} channel current upon transfection with SUR1Δ2. This led to inhibition of glucose-induced depolarization, calcium flux, insulin release and glibenclamide action. A non-mutagenic SNP on nucleotide position 333 (Pro69Pro) added another exonic splicing enhancer sequence detected by ASF/SF2, reduced relative abundance of SUR1Δ2 and slightly protected from non-insulin dependent diabetes in homozygotic individuals. Thus, SUR1Δ2 represents an endogenous K_{ATP}-channel modulator with prodiabetic properties in islet cells. Its predominance in heart may explain why high-affinity sulfonylurea receptors are not found in human cardiac tissue.

Keywords Sulfonylurea receptor · Alterative splicing · ATP-sensitive potassium channels · Glibenclamide · Glucose-induced insulin release

D. Schmid (✉) · M. Stolzlechner · A. Sorgner · A. Assinger · T. Moeslinger
Institute of Physiology, Center for Physiology and Pharmacology, Medical University of Vienna, Vienna, Austria
e-mail: diethart.schmid@meduniwien.ac.at

C. Bentele · P. Chiba
Institute of Medical Chemistry, Center for Pathobiochemistry and Genetics, Medical University of Vienna, Vienna, Austria

Introduction

Adenosine-5′-triphosphate-sensitive potassium channels (K_{ATP} channels) were originally discovered by Noma et al. [1] in metabolically inhibited cardiomyocytes. K_{ATP} channels are expressed as different isoforms not only in heart, but also in pancreatic islet cells, blood vessels, the brain and other tissues. The channels are voltage independent and ligand gated. In general, their open probability is increased in response to a drop in intracellular ATP or an increase in ADP [2]. It was concluded that they act as molecular sensors linking the metabolic state to the electrical activity of cells [3]. These channels are of particular importance for the signaling of glucose-induced insulin release of pancreatic beta cells [4].

K_{ATP} channels are octamers in their functional form, composed of four outer regulatory subunits, called sulfonylurea receptor 1 or 2 (SUR1, SUR2), and four inner pore-forming inward rectifier potassium channel subunits (Kir6.1 or Kir6.2) [5]. SUR1 and SUR2 are encoded by independent genes (ABCC8 and ABCC9), but nevertheless share sulfonylurea-receptor family signature sequences. In

addition, they both contain two nucleotide-binding domains (NBD1 and NBD2) and thus are members of the family of ATP-binding cassette (ABC) proteins [6].

Alternatively spliced human SUR2 mRNAs comprising either exon 39 or 40 were termed SUR2A and SUR2B [7]. The translated proteins differ in their sensitivity to nucleotides, tissue distribution and sensitivity towards the pharmacological modulator diazoxide [5]. Further SUR2 splice variants, human SUR2Δ14 [7] and SUR2Δ17 [8], have been identified. While SUR2Δ14 does not form a functional K_{ATP} channel, SUR2Δ17 confers a slightly reduced ATP sensitivity, because exon 17 codes for parts of the first nucleotide binding fold [8]. Even though these splice variants have been detected in rat and human tissue, functional studies were performed with the rodent isoforms only.

Knowledge about human SUR1 splice variants is limited. SUR1Δ31 was identified in human tissues [9] in low amounts, and the homologous rat gene was used to demonstrate that it impedes K_{ATP} channels from trafficking to the surface when co-expressed with Kir6.2. It displays a greatly reduced affinity for the sulfonylurea glibenclamide [9]. Four additional SUR1 splice variants were reported in guinea pig tissues [10].

Glibenclamide and other anti-diabetic sulfonylurea drugs have been suspected to block cardioprotective K_{ATP} channels in the myocardium even at therapeutic concentrations. Therefore, a controversy persists concerning whether sulfonylureas can exert harmful effects on the heart, especially in diabetic patients with coronary artery disease [11]. In this ongoing discussion, it has frequently been pointed out that cardiac sulfonylurea receptors (SUR2A) have a much lower affinity for sulfonylureas compared to the pancreatic beta cells and the drugs would thus not have any adverse effect on the heart [12]. Recently, mRNA sequences of high affinity SUR1 have been detected in human cardiac tissue [13]; however, a high-affinity binding site has only been demonstrated in rat [14], but not in human myocardium. Therefore, we hypothesized that a splice variant of SUR1 may predominate in human heart, altering or abolishing the action of sulfonylurea drugs.

Several mutations in the SUR1 gene were identified that cause either congenital hyperinsulinism or certain rare forms of congenital diabetes [15–17]. However, the question of whether the presence of splice variants of SUR1 may influence the response characteristics of glucose-induced insulin secretion has not been addressed.

The present study identified a novel abundant splice variant of SUR1 found in cardiac, pancreatic and other tissues of human origin, but not in rat tissues. This variant encoded for a truncated peptide lacking exon 2 that substantially changed the functional properties of K_{ATP} channels.

Materials and methods

Transcript scanning and tissue distribution RT-PCRs

All human and rat tissue RNAs were purchased from Clontech (Mountain View, CA). First strand cDNA synthesis was performed with 1 µg of total RNA using oligo(dT)18 primers and 200 units of a murine leukemia reverse transcriptase (RT) lacking intrinsic RNAse H activity (H Minus M-MuLV, Fermentas AG, St. Leon Rot, Germany) or a Primescript® RT enzyme (Clontech) at 42°C for 60 min. The enzyme was inactivated by increasing the temperature to 75°C for 5 min. For transcript scanning PCR, multiple exon-spanning primer pairs were designed using the academic freeware OligoExplorer1.2 (Gene-Link, Inc.) and custom synthesized (Biospring, Frankfurt am Main, Germany). The corresponding primer sequences and PCR product lengths are listed in Table 1. PCR was performed in a 50-µl buffer mix containing ammonium sulfate, 0.1 µg of cDNA, 200 µmol/l dNTPs, 1.5 mM $MgCl_2$, 1 µmol/l of each primer set and 1 unit of native Taq-DNA polymerase (Fermentas AG) or Advantage II® polymerase (Clontech). Cycle conditions were: 3 min initial denaturing at 95°C, 42 cycles of denaturing at 95°C for 30 s, annealing at 57°C for 1 min, elongation at 72°C for 1 min and a final elongation for 5 min. PCR products were visualized on agarose gels after staining with ethidium bromide and photographed. Relevant bands were cut out of the gel and purified using the Gel-Extraction Kit (Peqlab, Erlangen, Germany) with or without prior ligation and cloning into a pJET2.1_blunt vector (Fermentas AG) for subsequent custom sequencing (VBC-Biotech, Vienna Austria).

Relative abundances (r) of PCR products with two different molecular weights (MW_1 and MW_2) were calculated from their densitometric intensities (D_1, D_2) of photographed bands (ImageJ, NIH, USA) using the following formula:

$$r = \frac{\frac{D_1}{MW_1}}{\frac{D_1}{MW_1} + \frac{D_2}{MW_2}}$$

5′- and 3′-RACE-PCR

For 3′-RACE-PCR, cDNA template was derived from reverse transcription utilizing an anchor primer (for primer sequences, see Table 1). Nested PCR was performed with 3′GSP1 and 3′GSP2 as forward primers and an AUAP as the reverse primer for the first and second PCR round, respectively. For 5′-RACE-PCR, reverse transcription was carried out using a 5′GSP1 on exon 5. cDNA/RNA hybrids were digested using RNAse H and released fragments using RNAse T1. Subsequently, first strand cDNA was

Table 1 Primer sequences used in transcript scanning RT-PCR, 5′RACE-, 3′RACE- and tissue distribution RT-PCRs with lengths of corresponding amplicons obtained for regularly and alternatively spliced human SUR1

Detected cDNA (primer name)	Forward primer (5′-3′)	Reverse primer (5′-3′)	PCR prod. length[b] (bp)	PCR prod. length (bp)[b], alt. spliced
Transcript scanning RT-PCR				
SUR1 (EX 1- EX 5)	TCATCACCTTCCCCATCCTC	GCGTTCATCCACCAGTAG	583	441 (SUR1Δ2)
SUR1 (EX 6- EX 12)	TTGGGAAGGAGAACGACG	TGGACAGCAGGAACAGCG	804	
SUR1 (EX 13- EX 21)	CCCATGAGCCCACACCTC	GCGTTGACCACCAGACAG	626	
SUR1 (EX 22- EX 28)	GGGACGACAAGAGGACAG	GGATGAAGTAGCACACGATGG	903	
SUR1 (EX 29- EX 36)	CACACTTTGCCGAAACCGTAG	ATCTGAGCACTTCCTCTC	740	626 (SUR1Δ31)
SUR1 (EX 37- EX 39)	CGATGCCATCATCACAGAAG	CTGAGCAGCTTCTCTGGCTT	291	
5′-RACE-PCR				
SUR1 EX 5 (5′GSP1) (first strand)		GTTGGTAGTTGGTGAG		
Oligo dG-inosine anchor primer (second strand)	GGCCACGCGTCGACTAGTA CGGGIIGGIIGGGIIG			
SUR1 EX 5 (5′GSP2)	AUAP[a]	GCGTTCATCCACCAGTAG		
SUR1 EX 3 (5′GSP3)	AUAP[a]	GTGACAGCAGCCATGAAC	518	345 (SUR1Δ2)
3′-RACE-PCR				
Oligo dT anchor primer (first strand)		GGCCACGCGTCGACTAGTA CTTTTTTTTTTTTTTTT		
SUR1 EX 37 (3′GSP1)	CGATGCCATCATCACAGAAG	AUAP[a]		
SUR1 EX 39 (3′GSP2)	AAGCCAGAGAAGCTGCTCAG	AUAP[a]	137	
Human and rat tissue distribution RT-PCR				
hSUR1 (EX1–EX 3)	TCACCTTCCCCATCCTCTTC	GGTGACAGCAGCCATGAAC	233	91 (SUR1Δ2)
r/mkSUR1 (EX1–EX 4)	TCTTCATCACCTTCCCCATCCTC	CCTCCACAAGCAGCAGCATC	441	299 (rSUR1Δ2)

[a] *AUAP* Abridged universal anchor primer, GGCCACGCGTCGACTAGTAC

[b] Actual lengths of sequenced PCR products are given

purified to remove primers and enzymes using the Cycle Pure Kit (Peqlab). For tailing, terminal deoxynucleotidyl transferase (tdT, Fermentas) was used with either dATP or dCTP as the substrate. Tailed cDNA was used as a template for second strand cDNA synthesis using an M-MuLV-reverse transcriptase primed with oligo dT- or oligo dG-inosine anchor primers. A second purification step yielded the template for a two-step nested PCR. For the first round, UAP and 5′GSP2 primers were used, followed by a second round using UAP and GSP3 primers. Some 5′-RACE-PCR products were reamplified by PCR using the primer pair ATGCCCCTGGCCTTCTG/GTGACAGCAGCCATGAAC for sequencing.

Expression vectors for hSUR1Δ2, hKir6.2, and hSUR1

Full length open reading frames (ORFs) were amplified by PCR from human heart cDNA with the oligonucleotide primer pairs ATGCCCCTGGCCTTCTG and TCACCCA ATGAAGAGGATGG for SUR1Δ2 and ATGCTGTCCCG CAAGG and TCAGGACAGGGAATCTGGAG for Kir6.2, respectively, using a proofreading Phusion DNA-Polymerase (Finnzymes, Espoo, Finland). Amplified cDNA fragments of 153 and 1,173 bp, respectively, were isolated from a 2% agarose gel and cloned into pJET2.1_blunt vectors. Correct insert orientation was confirmed by SapI digestion (Kir6.2). SUR1Δ2 and Kir6.2 cDNAs were excised from the pJET2.1_blunt plasmids by digestion with the restriction enzymes NotI and XbaI I and ligated into the expression vectors, pcDNA3.1(+)_neo and pcDNA3.1 (+)_hygro (both from Invitrogen, Carlsbad, CA), respectively. For protein expression and co-immunoprecipitation studies, SUR1Δ2 ORF was subcloned into a pSecTag2B_ zeo vector (Invitrogen) within a NheI/EcoRI cassette in order to add a spacer and a tandem c-myc-His-tag. The expression vector for hSUR1 was obtained by subcloning the full SUR1-ORF of an artificially synthesized pENTR-ABCC8 entry vector (GeneCust, Dudelange, Luxembourg) into the pcDNA3.1(+)_hygro vector as a AflII/XbaI cassette.

Cell culture and transient transfections

RINm5F rat insulinoma cells were obtained from the American Type Culture Collection (ATCC, catalogue no.: CRL-11605™) and maintained in modified RPMI1640 medium supplemented with 10% FCS, 2 mM sodium pyruvate and 20 mM Hepes. Cells were used in low passage numbers to retain glucose responsiveness. COS-7 cells were cultivated using DMEM supplemented with 10% FCS. The cells were plated in petri dishes at a density of 30% and incubated for 12 h prior to transfection; 0.5 μg/ml of plasmid constructs was transfected using 2.5 μl/ml Lipofectamine-2000 (Invitrogen) according to the manufacturer's recommendations. In order to control for variations in transfection efficiency, 0.25 μg/ml of a pcDNA3.1 vector containing GFP was occasionally co-transfected. Successful transfection was confirmed by RT-PCR of DNAase-treated RNA and/or by Western blot.

Co-immunoprecipitation, Western blot

Forty-eight hours after transfection, 100-mm petri dishes, each containing approximately 2×10^7 cells, were washed with PBS and incubated in extracellular buffer in the presence of 10 mM glucose at 37°C for 30 min. Thereafter, cells were homogenized by an Ultraturrax (IKA, Staufen, Germany) in 150 mM NaCl, 10 mM TRIS-HCl, 1% Triton-X-100, pH = 7.4, ice cold lysis buffer supplemented with EDTA-free protease inhibitor cocktail (ROCHE, Vienna, Austria) with 5 mM Na_2ATP. Homogenates were spun down for 10 min at 500 g to remove debris. Each milliliter of whole cell lysate was co-immunprecipitated with 30 μl protein A-Sepharose beads (GE Healthcare, Munich, Germany) preloaded with 2 μg anti-Kir6.2 antibody (H-55, Santa Cruz Biotechnology, CA) before elution by boiling in sample buffer for 5 min. Precipitated proteins were separated on 18% Tris-Tricine gels and blotted onto PVDF-membranes (Immobilon-PSQ, Millipore, Schwalbach, Germany). Immunodetection was performed with a mouse anti-c-myc-tag antibody (Applied Biological Materials Inc., Richmond, Canada) at a 1:1,000 dilution in TBST. Anti-mouse HRP-conjugated antibody (GE Healthcare, Munich, Germany) was used as a secondary antibody at a dilution of 1:5,000. Finally, the blots were incubated with ECL Substrate (Pierce), and images were acquired on a chemiluminescence imager (Alpha Innotech, San Leandro, CA).

For detection of endogenous SUR1Δ2 in human tissue extracts (Biochain, Hayward, CA), the immunogenic peptide N-HSAAYRVDQGVC-C was chemically synthesized and coupled at the terminal cysteine residue to keyhole limpet hemocyanin (KLH). Two rabbits were immunized four times each 2nd week (Genscript, Piscataway, NJ). The IgG fractions of the anti-sera obtained from final bleeds as well as of the pre-immune sera were obtained by protein-A column chromatography (GE Healthcare) and used for Western blotting at a concentration of 20 μg/ml prior to anti-rabbit HRP-conjugated antibody (GE Healthcare) at a dilution of 1:5,000 (both in TBST).

Flow cytometry

Forty-eight hours after transfection, medium was removed from six-well plates, and COS-7 cells were detached by incubation in PBS/0.2% EDTA for 15 min at 37°C with

constant agitation. Cells were pelleted at 250 g for 5 min and incubated in a 100 µg/ml solution of the proprietary N-terminal polyclonal anti-SUR1 IgGs (as described in the previous paragraph) in PBS for 30 min. Cells were washed twice with PBS and incubated with 10 µg/ml anti-rabbit-FITC/PBS for 30 min. After the final wash, cells were resuspended in PBS/3% *p*-formaldehyde and subjected to flow cytometry (FACS Calibur™, Becton-Dickinson, Schwechat, Austria). Viable cells were gated in the FCS/SSC scattergram, and FL1-fluorescence histograms were analyzed for their mean fluorescence using CellQuest™ software (Becton-Dickinson).

Surface biotinylation experiments

Surface expression of SUR1 was assessed using surface biotinylation of primary amines (lysine residues) and streptavidin bead pull down. Briefly, transfected COS-7 cells were grown to confluence, the medium removed, and cells were washed twice with ice-cold PBS before incubation with 250 µg/ml biotin disulfide *N*-hydroxysulfosuccinimide ester (Pierce Fisher Scientific, Vienna, Austria) in ice-cold PBS for 30 min on a rocking platform. The reaction was quenched by adding 500 µg/ml biotin in PBS. Cells were scraped from dishes, washed, resuspended in ice-cold lysis buffer and subjected to repeated 5-s sonificatons within 30 min. Cell lysate was centrifuged at 10,000*g* for 2 min at 4°C, and the supernatant was loaded onto a spin column coated with NeutrAvidin™ agarose beads (Pierce) and incubated for 60 min. After centrifugation and washing steps, proteins were eluted following a 60-min incubation with 50 mM DTT, mixed with Laemmli buffer, and subjected to separation by 7% PAGE and Western transfer. After blocking, blots were incubated for 60 min with a 1:200 dilution of an anti-SUR1 antibody (C-16 or H-80, Santa Cruz Biotechnology) in TBST and an anti-goat or anti-rabbit HRP-conjugated antibody (GE Healthcare) at a dilution of 1:1,000 in the second step.

Patch-clamp experiments

Whole-cell voltage-clamp recordings were performed at room temperature. Fire-polished patch pipettes were prepared from 1.2-mm (outer diameter) borosilicate capillary glass (GC120F-10, Harvard Apparatus, Kent, UK) on a horizontal micropipette puller (Model P-87, Sutter Instruments, Novato, CA). The patch electrodes had an open tip resistance of 3–7 MΩ. Tight seals (>1 GΩ) were obtained with the transfected cells before break-in. The access resistance and membrane capacitance during recording varied from 7–30 MΩ and 3–13 pF, respectively. For capacitance compensation and current recording, an Axopatch 200B patch clamp amplifier was used (Axon Instruments, Foster City, CA). Current signals were low pass filtered (2 kHz; Bessel; four-pole filter, −3 dB), digitized (20 kHz, 16-bit resolution) and stored on a computer disk for later analysis with the pCLAMP 9 software (Axon Instruments). The bath medium contained 104 mM NaCl, 5.3 mM KCl, 0.8 mM $MgSO_4$, 5.6 mM Na_2HPO_4, 0.42 mM $CaNO_3$, 25 mM Na-HEPES (pH = 7.4) and 11.1 mM glucose. The intracellular pipette solution was composed of 140 mM KCl, 10 mM NaCl, 1.2 mM $MgSO_4$, 1.2 mM K_2HPO_4, 1 mM KEGTA and 10 mM K-HEPES, (pH 7.2). Na_3ATP was added in different concentrations (see "Results").

Inside-out excised patch experiments for single channel recordings were performed using standard procedures [18]. In these experiments, fire-polished patch pipettes had resistances between 3 and 6 MΩ. The pipette solution contained: 142 mM KCl, 2.8 mM NaCl, 10 mM KHEPES and 1.25 mM $CaCl_2$, pH = 7.4 adjusted with KOH. The bath solution was the calcium-free pipette solution supplemented with 1 mM EGTA, 0.5 mM $CaCl_2$ and HCl (pH = 7.3). MgATP was added at different concentrations from 0.01 to 3 mM. Pipette tip voltage was kept constant at 60 mV (corresponding to a membrane voltage of −60 mV). Current signals were digitized using a sampling frequency of 2 kHz and were digitally filtered using a 200 Hz Gaussian low pass filter. Open probability (Np_o) was computed using the following equation after fitting single channel opening events into the filtered current traces using Clampfit 9.2 software (Axon Instruments):

$$\mathrm{Np_o} = \frac{1}{T}\sum n_i \cdot t_i$$

whereby N is the number of channels in the patch (estimated from the highest current level in absence of ATP), and p_o is the open probability of a single channel, T is the recording time, n_i is the current level of an event (in multiplies of the single channel current), and t_i is the time the event stayed at its current level.

For quantification of ATP sensitivity, a Hill equation was fitted to the concentration-dependent $Np_o([ATP])$ values normalized to the $Np_o(0)$ value of the same patch measured without ATP in the bath solution:

$$\frac{\mathrm{Np_o}([\mathrm{ATP}])}{\mathrm{Np_o}(0)} = 1 - \frac{[\mathrm{ATP}]^n}{[\mathrm{ATP}]^n + k_i^n}$$

where n is the Hill coefficient and k_i is the half maximum inhibition constant.

Fluorescent measurement of membrane potential and intracellular $[Ca^{++}]$

Membrane potential was assessed using the fluorescent dye DiBAC4(3) (Molecular Probes, Eugene, OR). Monolayers of cells were washed with and incubated in extracellular

buffer consisting of 140 mM NaCl, 4.7 mM KCl, 1.2 mM $MgSO_4$, 1.2 mM K_2HPO_4, 1.25 mM $CaCl_2$, 10 mM Na-HEPES (pH = 7.4), 3 mM glucose and 100 nM of DiBAC4(3) at 30°C for 90 min. Cells were mounted on the stage of a modified Olympus IX50 inverted epifluorescence microscope and superfused with buffer at a rate of 2.5 ml/min (30°C). Fluorescence was excited every 5 s for a period of 100 ms with a 100-W Super High Pressure Mercury Lamp (USH 102D, Ushio, Japan) at 480 ± 20 nm utilizing a computer-controlled shutter (Uniblitz), and fluorescence was collected in real time at 535 ± 25 nm with a photomultiplier tube (Sequoia-Turner Model 450). Signals were amplified, acquired and stored on a personal computer using a self-designed Labview®-based data acquisition software tool (National Instruments, Austin, TX). At the end of each experiment, cells were fully depolarized with 30, 60 and 150 mM KCl to obtain maximum fluorescence (f_{max}) for calculation of the absolute membrane potential (Vm) using the Nernst equation [19]:

$$Vm = -\frac{RT}{F}\ln\frac{f_{max} - f_{min}}{f - f_{min}}$$

where R is the universal gas constant, T is absolute temperature, F is the Faraday constant, f_{min} is the autofluorescence, and f is the actual fluorescence.

In glibenclamide experiments, three-parameter Hill-type concentration response curves were fitted to datapoints by non-linear least square regression analysis using SigmaPlot11.0 (Systat Software, Chicago, IL).

For measurement of cytosolic [Ca^{++}], cells were loaded with 2 μM FLUO-4 acetomethylester (Molecular Probes) at room temperature for 30 min, washed with extracellular buffer, mounted on the microscope stage and superfused with buffer at 30°C. At the end of each experiment, cells were subjected to 30 mM KCl and subsequently to calcium-free extracellular buffer supplemented with 1 mM K_2EGTA/2 μg/ml ionomycin for obtaining F_{max} and F_{min}, respectively, to allow comparison of independent experiments.

Insulin secretion

Forty-eight hours after transfection, RINm5F cells were washed twice with PBS and preincubated for 1 h in extracellular buffer without glucose at 37°C. During a 30-min incubation period, insulin release and secretion were measured in extracellular buffer without glucose or in the presence of various glucose concentrations (2.5, 5, 10 and 20 mM) and complementing mannose concentrations for maintaining constant osmolarity. Thereafter, the cell supernatants were carefully removed and gently centrifuged to delete detached cells. Insulin was determined by a sensitive radioimmunoassay (DRG Instruments GmbH, Marburg, Germany) using a rat insulin standard and normalized to total protein content of the cells.

Chemicals

Unless otherwise stated, all chemicals were from Sigma-Aldrich (Vienna, Austria).

Results

Transcript scanning

The entire human SUR1 cDNA from human heart, including the 5′- and 3′-untranslated regions (UTRs), was systematically screened for alternative splicing of its constituent 39 exons. In order to achieve this, we employed a transcript scanning approach developed recently for the identification of multiplex splice variants of human brain T-type calcium channel alpha1 subunits [20]. We designed multiple RT-PCR primer pairs (see Table 1) for amplification of adjacent cDNA segments in order to reduce the chances of overlooking even small size differences of products in DNA-gel electrophoresis. Products were subsequently sequenced. The amplified cDNA segments consisted of sequences from exons 1–5, 6–12, 13–21, 22–28, 29–36 and 37–39 (Fig. 1b). Additionally, we employed 5′- and 3′-RACE-PCR to scan for variants truncated at either end. The strategy verified the presence of the SUR1Δ31 splice variant in a weak second band of 629 bp (Fig. 1c, third gel, 5th lane), which has been previously reported to be present in human heart [9]. In addition, amplification of the heart cDNA sample P1 with primers on exons 1 and 5 revealed a single, however, shortened PCR product of 441 bp (Fig. 1c, third gel, 1st lane), which is 142 bp smaller than the expected size (583 bp) of regularly spliced SUR1. Nevertheless, products of expected size appeared in some heart cDNA samples (P2, P3, second gel) as weak second bands. Sequencing uncovered the shorter, abundant amplicon to be a novel splice variant of SUR1 with an omitted exon 2 (SUR1Δ2) (Fig. 1d). Sequencing of 5′-RACE PCR products after terminal deoxynucleotidyl transferase (tdT)-mediated 5′oligo-dC tailing confirmed the presence of SUR1Δ2 in a 345-bp product, while tdT-mediated 5′oligo-dA tailing revealed regular SUR1 in a 518-bp 5′-RACE product and an additional shorter product (244 bp) lacking exon 1 and the first six nucleotides of exon 2 (Fig. 1c, first gel). The latter might be present because of a prematurely interrupted reverse transcription [21]. 3′-RACE-PCR produced single bands that were identical to the 3′ terminus of regular SUR1 cDNA (Fig. 1c, fourth gel).

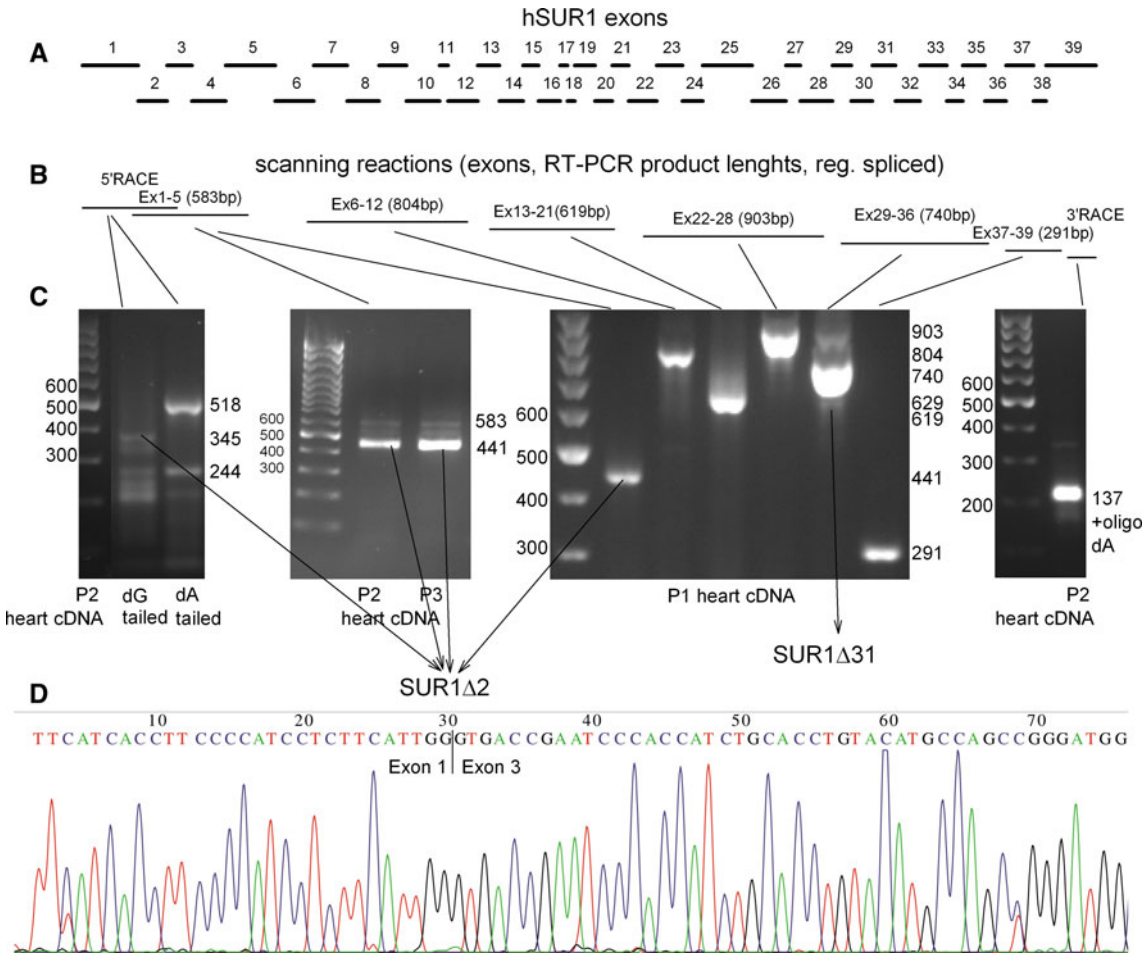

Fig. 1 Transcript scanning RT-PCRs and 3′- as well as 5′-RACE-PCRs for systematic detection of alternatively spliced SUR1 mRNA variants in human hearts (templates: cDNAs from individuals P1-P3). **a** Exons of regularly spliced hSUR1 mRNA indicated in representative lengths. **b** Localizations of RT-PCR scanning reactions relative to exons and expected PCR-product lengths (of regularly spliced SUR1). **c** Photographs of DNA gel electrophoresis for size differentiation of the PCR-products, all of which were subsequently sequenced. *First gel*: 5′RACE-PCR after terminal deoxynucleotidyl transferase (tdT)-mediated oligo-dG tailing of P2 cDNA reveals SUR1 lacking exon 2 (SUR1Δ2, 345 bp; the bands below are unspecific amplification products). 5′RACE-PCR following tdT-oligo-dA tailing leads to the detection of regularly spliced SUR1 (518 bp) and a SUR1 transcript lacking exon 1 and the first six nucleotides on exon 2 (244 bp). *Second gel*: Exon 1–5 RT-PCR using cDNA from individuals P2 and P3 shows SUR1Δ2 (441 bp) and concomitant SUR1 (583 bp) as a weak second band. *Third gel*: All scanning reactions using cDNA from P1 with exclusive SUR1Δ2 expression (441 bp) in the exon 1–5 reaction and the previously [9] identified SUR1Δ31 variant (629 bp) as a weak lower band in the Ex 29–36 reaction. *Fourth gel*: Results of 3′RACE-PCR. 100 bp ladders on the *left* of each gel. **d** A representative sequencing chromatogram for all four shortened PCR products obtained by three scanning reactions using primers on exons 1–5 as well as by oligo dG tailed 5′RACE-PCR with reverse primer on exon 3 confirming the lack of exon 2 and thus the SUR1Δ2 splice variant

Predicted SUR1Δ2 protein

Figure 2 depicts the consequence of the omission of exon 2 for the nucleotide and protein sequence of SUR1Δ2. Since exon 2 consists of 142 nucleotides, a number that is not divisible by 3, lack of exon 2 causes a frame shift for protein translation. The last two nucleotides of exon 1 (GG) and the first nucleotide of exon 2 (A) form a codon for glycine in SUR1. The first four nucleotides of exon 3 are GTG A. Omission of exon 2 puts the codon TGA into a reading frame (GGG TGA), generating a stop codon immediately after a GGG encoded glycine residue in the SUR1Δ2 splice variant (Fig. 2b).

For prediction of the secondary structure and membrane topology, the peptide sequence was submitted to the PSIPRED Protein Structure Prediction Server [22] and the NetNGlyc Server (http://www.cbs.dtu.dk/services/NetNGlyc/). The predictions indicated a transmembrane helix with an outside and inside helix cap and an N-terminal extracellular coil (Fig. 2c) with an intermediate strength N-linked glycosylation site at position 10 (NHS, signal sequence).

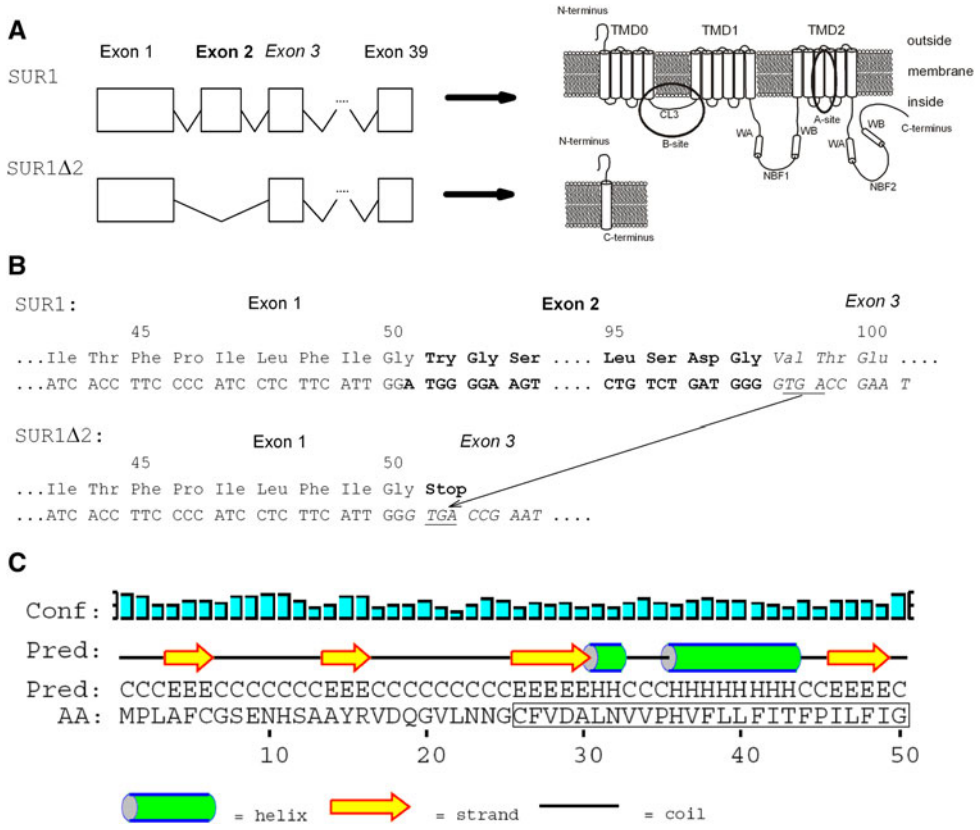

Fig. 2 Prediction of the truncated peptide structure of SUR1Δ2. **a** Exon sequence and accepted topology of SUR1, redrawn after [5, 38], in comparison with the putative structure of SUR1Δ2, which lacks nucleotide-binding domains and sulfonylurea binding sites. TMD0-2: Transmembrane domains 0–2, A- and B-sites: bi-partite model of the sulfonylurea binding site according to [38]; parts of the B-site on Kir6.2 pore forming unit are not shown. CL3: Connecting loop 3, *WA* and *WB* Walker A and B motifs, *NBF* nucleotide binding folds. **b** Amino acid and cDNA sequences of SUR1 and the consequences of omission of exon 2. Parts of the sequences of exon 1 (*normal font*), exon 2 (*bold font*) and exon 3 (*italic font*) are shown. The *arrow* indicates the position at which a TGA stop codon is generated by a frameshift in the SUR1Δ2 splice variant. **c** Secondary structure of SUR1Δ2 predicted by the PSIPRED protein structure prediction server [22], *Conf* confidence level of prediction (0–9), *Pred* predicted substructures: *C* coil, *E* strand, *H* helix, *AA* full amino acid sequence of SUR1Δ2. Enclosed in rectangle: sulfonylurea receptor signature sequence motif I-2

Tissue distribution of SUR1Δ2 mRNA in human and rat tissues

Figure 3a shows the results of RT-PCR analyses of a Clontech RNA panel containing 21 major human tissues. Exon 2 spanning primers on exon 1 and 3 of human SUR1 were used. cDNA was synthesized with oligo-dT primed reverse transcriptase. The simultaneous presence of SUR1 and SUR1Δ2 mRNA was detected in human pancreas, adult and fetal brain, prostate and spinal cord, whereby the relative abundance of SUR1Δ2 compared to regularly spliced SUR1 was lowest in pancreas (Fig. 3d). An almost exclusive SUR1Δ2 expression (more than 80%) was found in heart, skeletal muscle, kidney, testis and uterus. In contrast, bone marrow, fetal and adult liver, lung, placenta, spleen, thymus, trachea and small intestine lacked both SUR1 variants.

Figure 3b shows the results of RT-PCR analyses of an RNA panel containing eight major rat tissues. Exon 2 spanning primers on exon 1 and 4 of rat SUR1 were used. In contrast to human tissues, all tested rat tissues completely lacked expression of SUR1Δ2. Rat lung, heart (right and left ventricle), pancreas, cortex, medulla oblongata, liver and skeletal muscle expressed SUR1 only. The SUR1Δ2 peptide itself could be detected by immunoblotting in human brain extract using a proprietary rabbit IgG antibody raised against an antigenic peptide sequence between the gylcosylation signal sequence (NHS) and the outer helix cap (Fig. 3c). It appeared as a faint band at 5.6 kD and as dimeric and tetrameric complexes at 11 and 22 kD, respectively.

The relative abundance of SUR1Δ2 inversely correlated with spliceosome-specific ASF/SF2 alternative-splicing-factor expression in SUR1-containing tissues ($r = -0.79$, Fig. 3e). For this analysis, ASF/SF2 mRNA tissue expression data were taken from the Geneatlas transcriptome database [23] via BioGPS [24], dataset 211784_s_at and normalized to the expression of the constitutive splicing subunit U2ASF2 mRNA, dataset 218381_s_at.

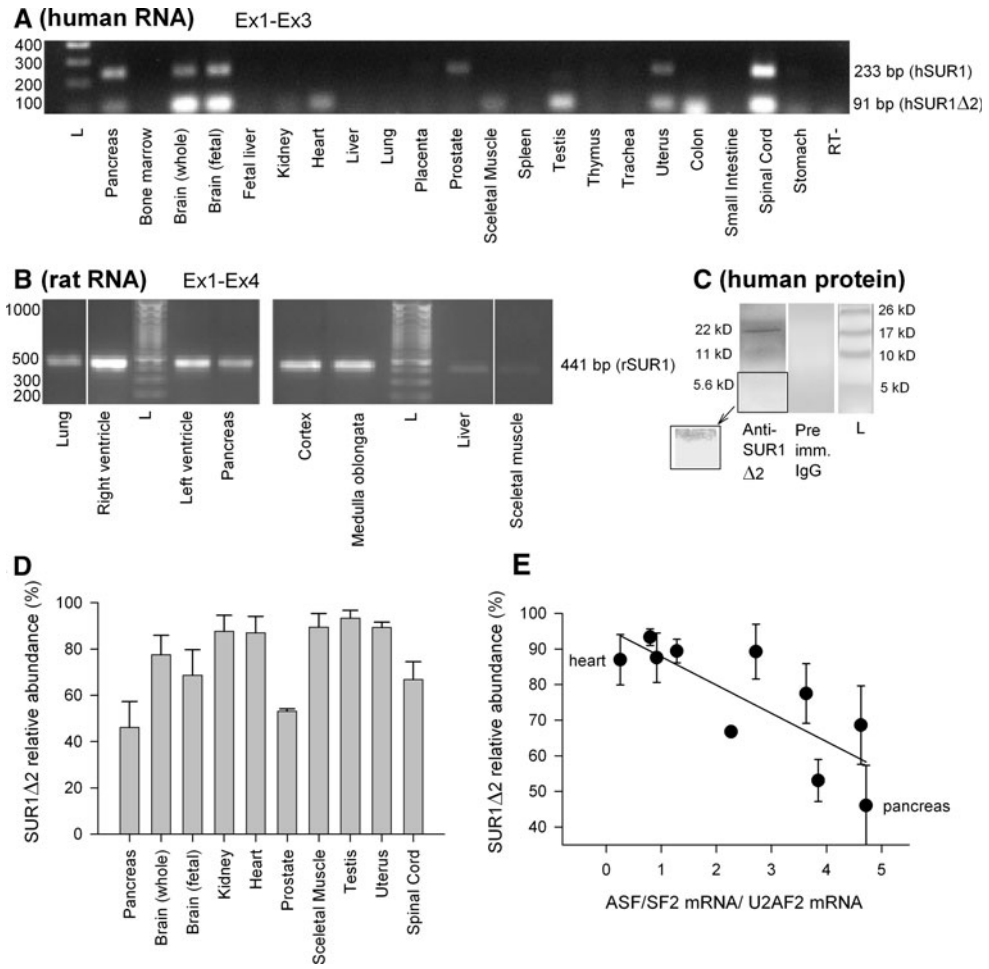

Fig. 3 Tissue distribution pattern of SUR1 and SUR1Δ2 expression. **a** RT-PCR using primers on exon 1 and 3 for analysis of the SUR1 (233 bp) and SUR1Δ2 (91 bp) transcripts in cDNAs of 21 human tissues obtained by reverse transcription of a Clontech RNA panel. **b** RT-PCR using primers on exon 1 and 4 for analysis of rSUR1 (441 bp) and rSUR1Δ2 (299 bp, not detectable) transcripts in cDNAs of eight rat tissues obtained by reverse transcription of a rat RNA panel. **c** Immunodetection of SUR1Δ2 in human adult whole brain extract. The first strip was probed with anti-SUR1Δ2 IgG, while the second strip was incubated with preimmune-IgG from the same rabbit. For easier visibility of the faint 5.6-kD band, the contrast in the lower portion of the first strip was enhanced as indicated by the *rectangular* region. **d** Densitometrically determined relative abundance of human SUR1Δ2 in relation to all SUR1 transcripts in tissues expressing SUR1 (means ± SEM of three independent RT-PCR experiments). **e** Inverse correlation between relative abundance of SUR1Δ2 mRNA and relative abundance of ASF/SF2 mRNA normalized to U2AF2 constitutive splicing factor in SUR1-containing tissues. The corresponding regression line is shown (regression coefficient $r = -0.79$). *L* ladders

Splice site probability predictions in human and rat ABCC8 genes

In order to reveal the genomic background for the existence of SUR1Δ2 in human tissues and to explain the lack of SUR1Δ2 in rats, the full gene sequences of human ABCC8 (Ensembl accession no.: ENSG00000006071) and rat Abcc8 (Ensembl accession no.: ENSRNOG00000021130) were submitted to the NETGENE server (http://www.cbs.dtu.dk/services/NetGene2/) for neural network prediction of splice donor and acceptor site probabilities [24]. The predicted confidences of all detected sites within the first 13,000 nucleotides are shown in comparison to the predicted probability of the actual splice sites for both human (Fig. 4a, b) and rat (Fig. 4c, d) donor and acceptor sites. All actual splice donor and acceptor sites had a probability close to or greater than the predicted cutoff level for strong splice sites. However, the first actual splice acceptor site in human ABCC8 (indicated by an arrow in Fig. 4b) had a markedly lower probability (0.77) than the corresponding first actual splice acceptor site in the rat gene (0.96). Exon 2 in human ABCC8 therefore represents a weak exon with susceptibility for alternative splicing (cutoff probability value for obligatory sites ≥0.90).

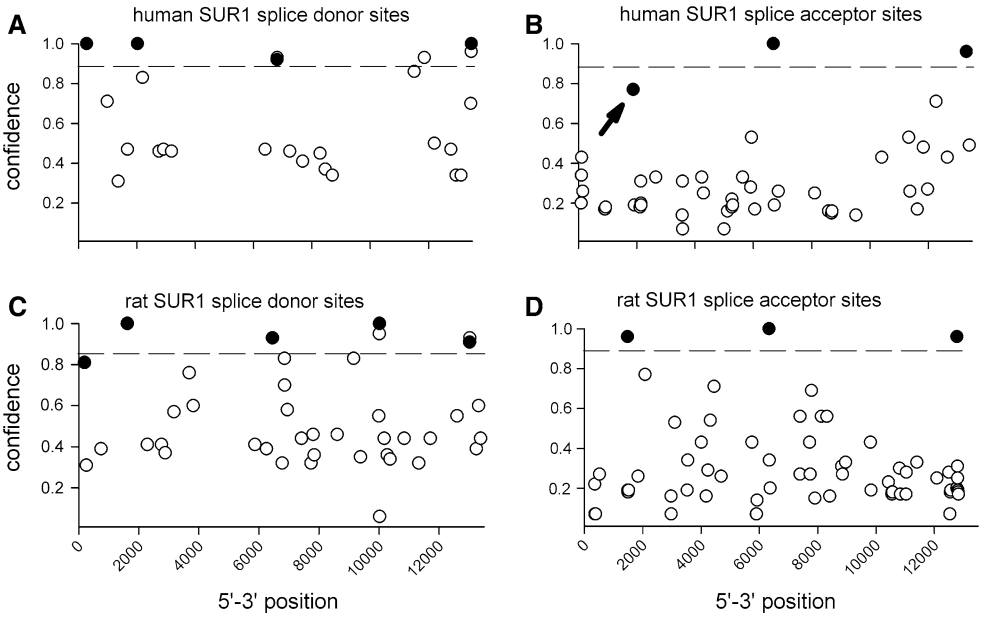

Fig. 4 Neural network bioinformatic prediction of splice donor (**a**, **c**) and splice acceptor site probabilities (**b**, **d**) in human ABCC8 (**a**, **b**) and rat Abcc8 genes (**c**, **d**) using NETGENE 2 server [24] within the first 13,500 bases. *Horizontal dashed lines* indicate the predicted cutoff level of confidence for strong splice sites. Confidences of confirmed actual sites are depicted as *filled circles*, others as *open circles*. The *arrow* shows the reduced splice acceptor site probability of the first actual acceptor site of human ABCC8 preceding exon 2. *Note*: NETGENE 2 failed to predict the third (out of four) actual splice acceptor site in the rat Abcc8 gene for unknown reasons

Recombinant expression of SUR1Δ2 and co-immunoprecipitation with KIR6.2

For expression and functional studies, the human SUR1Δ2 open reading frame (ORF) was cloned from human heart cDNA and subcloned into mammalian expression vectors. A spacer and a c-myc/His tag were introduced at the C-terminus of SUR1Δ2 leading to a predicted molecular weight for the fusion peptide of about 10 kD. COS-7 cells were selected as a heterologous expression system, because they have only a negligible background expression of SUR1 mRNA (Fig. 5a) or protein (Fig. 5e, f). Thus COS-7 cells were triple transfected with hKir6.2, hSUR1 and SUR1Δ2-cmyc to both allow trafficking of Kir6.2/SUR1 channels to the membrane by masking the RKR endoplasmic reticulum (ER) retention sequences [25] and to investigate whether SUR1Δ2 interacts with Kir6.2 in these complexes. As shown in Fig. 5b, immunoblot detection of the SUR1Δ2 c-myc peptide in the input extract revealed two major bands of approximately 13 and 17 kD, and a faint band at 10 kD. The 17-kD protein was the *N*-glycosylated form of SUR1Δ2, since peptide-*N*-glycosidase F (PNGase F) digestion left a single 10-kD band corresponding to the non-glycosylated SUR1Δ2. The 13-kD band appeared in the Kir6.2-precipitate, suggesting a direct physical interaction between partly glycosylated SUR1Δ2 and Kir6.2.

Surface expression of SUR1Δ2 and SUR1

In order to investigate whether SUR1Δ2 reaches the plasma membrane and how this may be modified by the presence of Kir6.2 and/or SUR1, we performed flow cytometric surface expression experiments. A proprietary antibody directed against a peptide sequence common to SUR1/SUR1Δ2 near their N-terminus (N-HSAAYRV DQGV-C) was used for labeling of intact COS-7 cells. Cells transfected with SUR1Δ2 alone displayed a significant right shift in the fluorescence histogram compared to mock-transfected cells (Fig. 5c). In contrast, cells transfected with SUR1 required the presence of Kir6.2 to show a significant surface expression signal (Fig. 5d). This indicated that SUR1Δ2 reaches the plasma membrane by itself—in the absence of Kir6.2. However, when SUR1Δ2 was co-transfected with Kir6.2, a marked reduction of the SUR1Δ2 surface appearance was observed. Triple expression (SUR1Δ2, SUR1, Kir6.2) resulted in a signal that was less than the sum of the isolated SUR1Δ2 and Kir6.2-mediated SUR1 surface expressions.

In order to differentiate between SUR1 and SUR1Δ2 surface expression in cells transfected with both forms, we performed surface biotinylation experiments and subsequent pull down of extracted plasma membrane proteins by streptavidin beads to assess the isolated SUR1 surface expression by Western blot with a C-terminal antibody (Fig. 5e). Again, only in the presence of Kir6.2, a significant expression of the membrane-bound glycosylated SUR1 (approximately 250 kD) could be detected. Triple expression with SUR1Δ2 caused a clear reduction of SUR1 by about 50% (Fig. 5e, f). A synopsis of data shown in Fig. 5d and f indicated the following: (1) the contribution of SUR1 to the height of the bar of SUR1/SUR1Δ2/Kir6.2 triple-transfected cells was approximately 5 of 13 RFU (rightmost bar in Fig. 5d). (2) The residual signal (8 RFU) could be attributed to SUR1Δ2, a value that was almost identical to that seen in samples in which a transfection

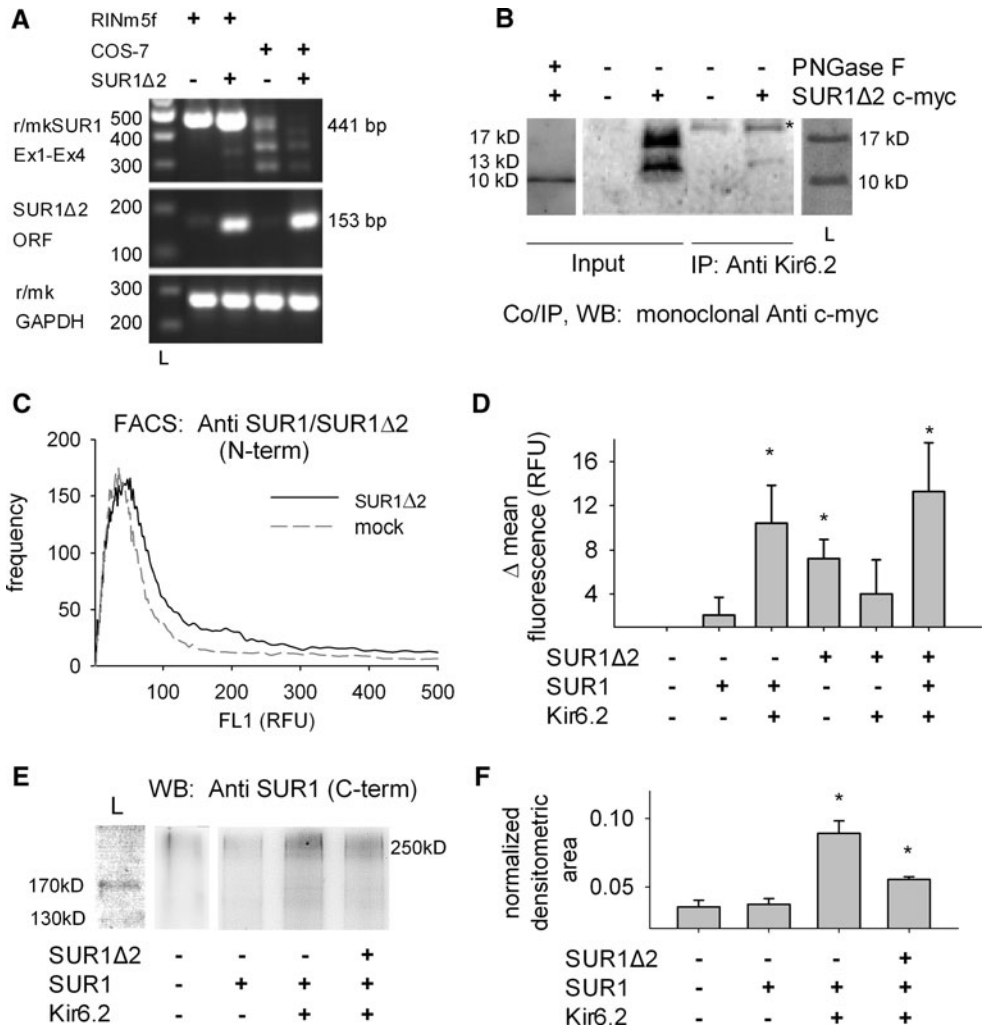

Fig. 5 Detection of SUR1Δ2 mRNA and protein in cells transfected with recombinant SUR1Δ2 cDNA, its physical interaction with Kir6.2 and SUR1Δ2/SUR1 surface expression. **a** RT-PCR of cDNA from pcDNA3.1_mock and pcDNA3.1_SUR1Δ2 transfected RINm5F and COS-7 cells using primers for rSUR1 (rat)/mkSUR1 (monkey) exon 1 and 4, human SUR1Δ2 open reading frame and r/mk (rat/monkey) GAPDH as the housekeeping gene. Wild-type RINm5f expresses rSUR1, but does not display endogenous SUR1Δ2. Wild-type COS-7 essentially lacks SUR1. **b** C-myc tagged SUR1Δ2 appears in three distinct forms: 10, 13 and 17 kD in the IP-input extracts. The physical association between the 13 kD form of SUR1Δ2 and Kir6.2 is demonstrated by co-immunoprecipitation (IP). COS-7 cells were triple transfected with pcDNA3.1_hKir6.2, pcDNA3.1_hSUR1, and pSeq_hSUR1Δ2-c-myc (+) or pSecTag2B_mock (−). IP was performed on Triton X-100/TBS solubilized COS-7 whole cell extracts using anti-Kir6.2 antibodies. Monoclonal anti-c-myc tag antibodies were used for subsequent Western blotting (WB). Extracts in *lane 1* were digested with peptide N-glycosidase F (PNGase F) prior to WB. The *asterisks* indicate 25-kD light chains of the precipitating antibody. *L* ladders. **c** Surface expression of SUR1/SUR1Δ2 assessed by flow cytometry (FACS) of intact COS-7 cells stained with an N-terminal SUR1/SUR1Δ2 antibody. Frequency distribution histogram of FL1 fluorescence of SUR1Δ2- and mock-transfected cells. **d** Statistics of flow cytometric mean fluorescences (FL1) in relative fluorescence units (RFU) of SUR1/SUR1Δ2/Kir6.2-transfected COS-7 cells stained as in subfigure **c** (mean fluorescence of mock-transfected cells was subtracted in each experiment). Mean ± SEM of $n = 4$–6 independent experiments for each group. *$p < 0.05$ (compared to mock-transfected group, Fisher's LSD). **e** Surface expression of glycosylated SUR1 (approximately 250 kD) assessed by Western blot of membrane proteins after surface biotinylation of COS-7 cells that were transfected as indicated (a C-terminal SUR1 antibody was used). **f** Densitometric evaluation of glycosylated SUR1 bands normalized to an unspecific band of $n = 4$ blots. *$p < 0.05$ (compared to mock group, Fisher's LSD)

with only SUR1Δ2 had been performed (Fig 5d, 4th bar from left). This suggested an essentially unimpeded trafficking of SUR1Δ2 to the cell surface in triple-transfected cells. (3) SUR1Δ2 reached the surface both in complex with Kir6.2/SUR1, but also independently: The residual SUR1Δ2 surface expression when co-expressed with Kir6.2 alone (3.5 RFU in bar 5 in Fig. 5d) and the difference in bars 3 and 6 of the same figure, which reflected the SUR1Δ2 fraction that reached the plasma membrane in a Kir6.2/SUR1 independent manner, were equal.

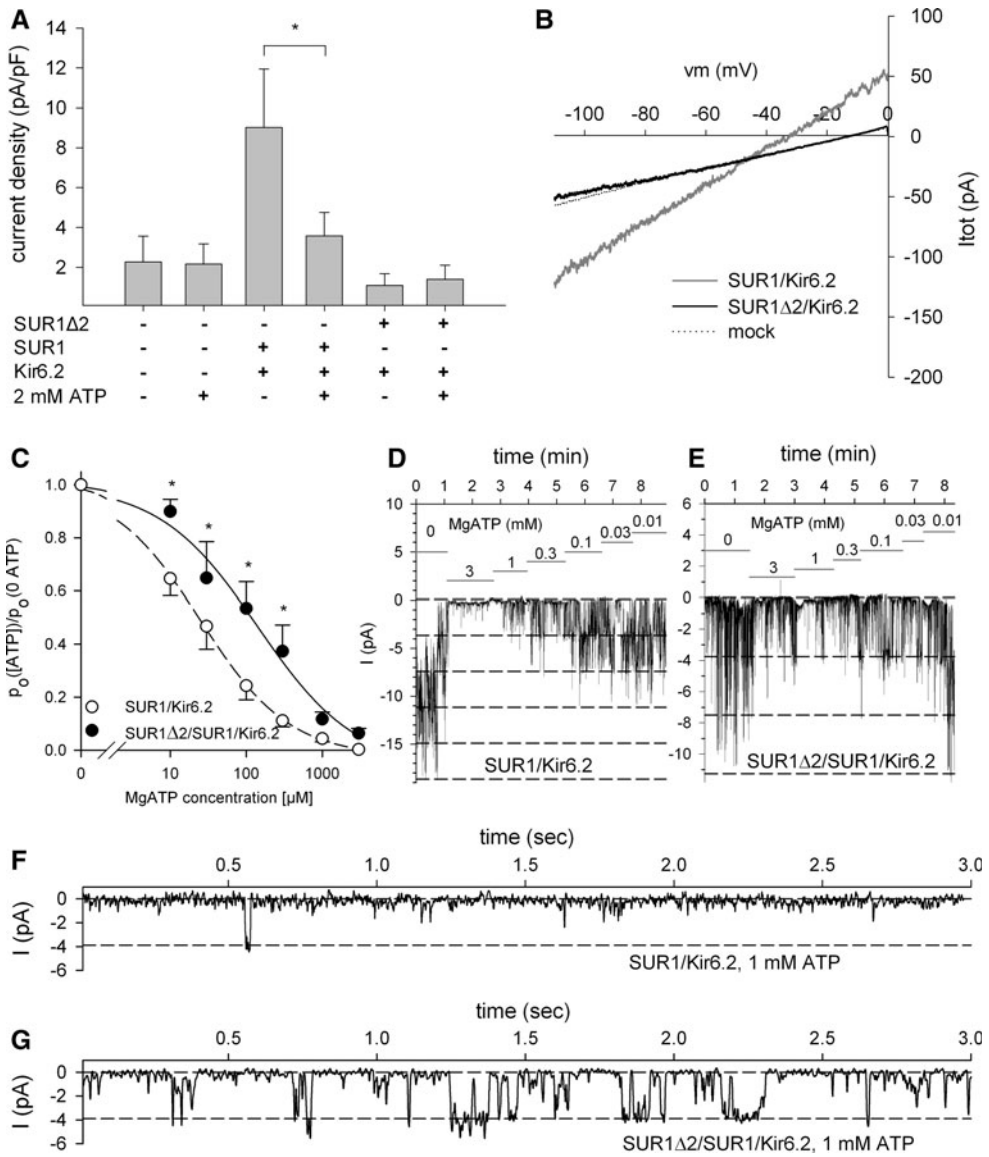

Fig. 6 SUR1Δ2 containing K_{ATP} channels expressed in COS-7 cells display a reduced ATP sensitivity. **a** Whole cell current densities measured 5 min after break-in at a holding potential of 0 mV. COS-7 cells were transfected as indicated. The pipette contained either 0 or 2 mM ATP. Mean ± SEM of $n = 4$ independent experiments for each group are shown. $^*p < 0.05$ (Student's t test). **b** Representative I/V curves of SUR1/Kir6.2, SUR1Δ2/Kir6.2 or mock-transfected COS-7 cells. The pipette contained no ATP when these traces were recorded. **c** MgATP dependence of the open probability (p_o) of single channels (normalized to p_o in the absence of MgATP) in inside-out excised patches from SUR1/Kir6.2 (*open symbols*: mean ± SEM, $n = 8$) or SUR1Δ2/SUR1/Kir6.2-expressing cells (*closed symbols*: mean ± SEM, $n = 3$–5). A Hill equation was fitted to the data points yielding a $K_i = 25.3 \pm 6.3$ μM for SUR1/Kir6.2 (*dashed line*) and $K_i = 141.0 \pm 9.1$ μM for SUR1Δ2/SUR1/Kir6.2 (*solid line*) containing patches. The Hill coefficients were 0.8 and 0.67, respectively. $^*p < 0.05$ between groups, Fisher's LSD). (**d**, **e**) Representative inside-out excised patch recordings with the indicated MgATP concentrations in the bath solution from SUR1/Kir6.2 (**d**, 5 channels) or SUR1Δ2/SUR1/Kir6.2 (**e**, 3 channels) containing patches clamped to −60 mV at symmetrical $[K^+]$ conditions. *Horizontal dashed lines* show integer multiples of mean single channel currents. (**f**, **g**) Single channel events in SUR1/Kir6.2 and SUR1Δ2/SUR1/Kir6.2 containing patches at a MgATP concentration of 1 mM ATP. The single channel current was −3.9 pA at −60 mV holding potential (65 pS conductance) in both cases

Isolated SUR1Δ2 could not be detected by surface biotinylation with biotin disulfide *N*-hydroxysulfosuc cinimide ester, because SUR1Δ2 does not contain lysine residues in its extracellular sequence (data not shown).

Whole cell patch clamp experiments

In order to deal with the question of whether a possible association of SUR1Δ2 with Kir6.2 without SUR1 would lead to functional channel expression on the plasma

membrane, whole-cell patch clamp experiments with COS-7 cells were performed (Fig. 6a, b). Coexpression of SUR1 with Kir6.2, as expected, resulted in a current that was dependent on the ATP content in the pipette (0 vs. 2 mM ATP, measured 5 min after break in) and exhibited a slight inward rectified characteristic in the I/V curve (Fig. 6b). However, coexpression of SUR1Δ2 with Kir6.2 led to neither any current being higher than the background current of mock-transfected cells nor to any ATP dependency.

Inside-out excised patch recordings

Since SUR1 was partly replaced by SUR1Δ2 after association with Kir6.2, as shown above in the surface expression experiments, we were interested in assessing the ATP sensitivity of this hybrid SUR1Δ2/SUR1/Kir6.2 channel compared to normal SUR1/Kir6.2 channels. Single channel recordings were done after excising membrane patches from transfected cells and exposing the inner side to the bath solution containing different MgATP concentrations (Fig. 6d, e). Channel open probabilities (Np_o) were measured and normalized to the maximum value at zero ATP. The half maximum inhibition constant (k_i) for SUR1/Kir6.2 channels was 22.4 ± 1.1 μM, which is in agreement with previously published values [26], whereas k_i values for SUR1Δ2/SUR1/Kir6.2 hybrid channels were 141.0 ± 9.1 μM, corresponding to an almost sixfold reduction in ATP sensitivity (Fig. 6c). Notably, even a high ATP concentration of 1 mM could not fully abolish single channel events in the hybrid channels (Fig. 6f, g). The single channel conductance of the hybrid channel, however, was unchanged, as indicated by 3.9 pA single channels currents (at −60 mV) in both kind of patches.

Functional consequences of SUR1Δ2 expression in insulinoma cells

RINm5F cells are rat insulinoma cells expressing functional K_{ATP} channels composed of rSUR1 and rKir6.2 [27]. RT-PCR analysis of DNAase-treated total RNA confirmed that mock-transfected cells lacked any SUR1Δ2 and transfected RINm5F cells in fact contained both rSUR1 and SUR1Δ2 mRNA (Fig. 5a). In order to investigate the effects of a concomitant presence of SUR1Δ2 on the functional properties of regular rSUR1 containing K_{ATP} channels, we co-transfected RINm5F cells with human SUR1Δ2 and green fluorescent protein expression vectors. Cells were bathed in an extracellular medium containing high glucose (11 mM) in order to maintain high intracellular ATP levels and thus low basal K_{ATP}-channel open probability. The potassium current recorded with 2 mM ATP in the patch pipette 10 min after obtaining a whole cell configuration in mock-transfected cells mostly reflected the activity of voltage-dependent potassium (Kv) channels (Fig. 7a). This current has typical activation kinetics and voltage dependence of the conductance as represented by the rising slope of the I-V relationship (Fig. 7b). With an ATP-free pipette solution, K_{ATP} currents increased in amplitude because of ATP diffusion from the cell interior into the patch pipette (Fig. 7c), reaching a maximum between 5 and 10 min before channel rundown [28]. However, when the intracellular pipette solution contained 2 mM ATP, the maximum increase in I_{KATP} measured at a holding potential of −35 mV remained much stronger in SUR1Δ2 than in mock-transfected cells. The statistical evaluation of maximum I_{KATP} currents normalized to cell capacitance (current densities) measured with different ATP concentrations in the intracellular solution is depicted in Fig. 7d. Results again indicated a reduced potency of ATP to close K_{ATP} channels in the SUR1Δ2-containing cells. Visually read off k_i values for ATP-induced channel inhibition in these whole cell experiments were much higher than shown before with excised patches. This was most probably due to the presence of ADP and other intracellular modulators. However, this type of experiment represented a more physiological situation.

Effects of SUR1Δ2 on glibenclamide-induced depolarization

Since the truncated SUR1Δ2 peptide did not contain any of the sulfonylurea receptor-binding sites of SUR1, but retained the ability to bind to the Kir6.2 K_{ATP} channel subunits, we were interested in whether and, if so, how SUR1Δ2 could alter sulfonylurea drug action. RINm5F cells were transfected with untagged SUR1Δ2 and subjected to fluorescent membrane potential measurements. Cells were loaded with 100 nM DiBAC4(3), a bis-oxonol, which is a membrane potential-sensitive dye that increases its fluorescence upon depolarization and strictly follows the Nernst equilibrium at this low concentration [19]. Following hyperpolarization of cells with 100 μM diazoxide, glibenclamide was added at 1, 3 or 6 nM (Fig. 8a, b). Depolarization was concentration dependent (Fig. 8c) and much weaker in SUR1Δ2 than in mock-transfected cells. A comparison of the concentration-response curves fitted to the two sets of data points shows that SUR1Δ2 did not alter the potency (close to 1.1 nM for both cell types), but strongly reduced the efficacy of glibenclamide to depolarize the membrane potential (by 7.7 mV in SUR1Δ2 vs. 29.5 mV in mock-transfected cells, Fig. 8c).

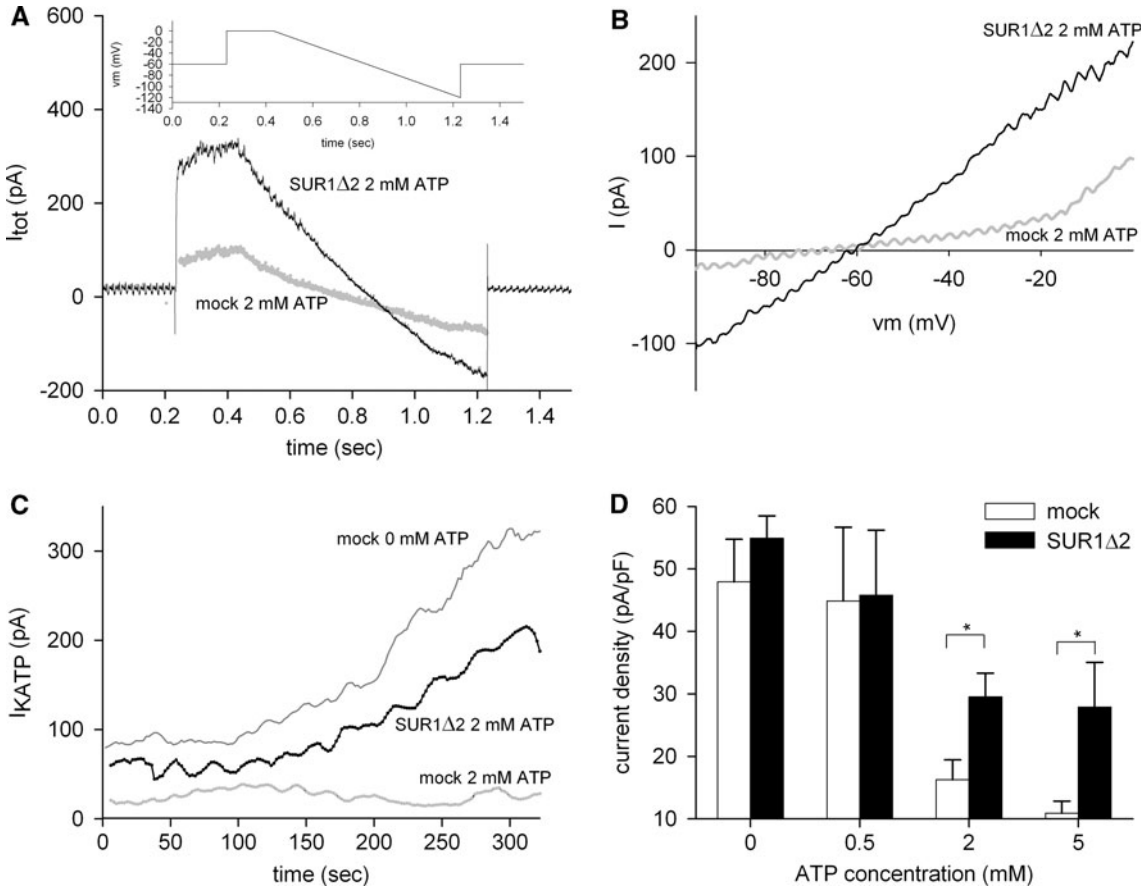

Fig. 7 Recombinant expression of SUR1Δ2 in rat insulinoma (RINm5F) cells activates K_{ATP} channels (whole cell patch clamp). **a** Voltage clamp and resulting currents: the currents were monitored every 2 s and elicited by the following voltage ramp protocol (inset to Fig. 6a): after an initial depolarizing step pulse to 0 mV for 200 ms from the holding potential of −60 mV, a negative ramp was applied from 0 to −120 mV with a constant speed of −0.120 V/s. Maximum currents (300 s after break-in) of SUR1Δ2 and mock-transfected cells with a pipette filled with 2 mM ATP are shown. **b** I-V relationship of potassium currents in SUR1Δ2 and mock-transfected cells in the presence of 2 mM ATP, 300 s after break-in. While in mock-transfected cells, voltage-dependent Kv conductance (*slope*) predominates, SUR1Δ2 induces a voltage-independent K_{ATP} conductance with a weak inward rectifier characteristic (I_{Kv} subtracted). **c** The time course of I_{KATP} development after break-in at −35 mV holding voltage in SUR1Δ2-transfected and mock-transfected cells in the presence and absence of 2 mM ATP (sliding means of 5 consecutive data points are shown). **d** ATP dependence (ATP in the pipette) of maximum I_{KATP} current densities developed at −35 mV holding potential. Mean ± SEM of $n = 4$–8 independent experiments for each group. *$p < 0.05$ (Fisher's LSD test was performed between SUR1Δ2 and corresponding mock groups)

Effects of SUR1Δ2 on glucose-induced depolarization—cytosolic [Ca^{++}] and insulin secretion of insulinoma cells

A shift from 3 to 10 mM glucose, which corresponds to a low normoglycaemic and a hyperglycaemic state in vivo, respectively, caused mock-transfected RINm5f cells to depolarize by 5.3 ± 0.3 mV ($p = 0.003$) from a resting potential of −51.4 ± 3.9 mV (Fig. 9a, b) within 20–30 min. In contrast, the stepwise increase in glucose concentration led to a slight hyperpolarization by −1.7 ± 2.7 mV in SUR1Δ2-transfected cells, which was, however, not always strong enough to be statistically significant (Fig. 9a, b).

Cytosolic [Ca^{++}] behaved similarly. Mock-transfected cells responded to a stepwise increase of glucose from 3 to 10 mM with a significant increase in [Ca^{++}] by 35 ± 4%, whereas SUR1Δ2-transfected cells reacted inversely with a drop by 21 ± 17% (Fig. 9c, d).

Insulin secretion data were analyzed using two-way ANOVA, which revealed that both increasing glucose concentrations ($p = 0.033$) and SUR1Δ2 transfection ($p < 0.001$) had a highly significant overall effect on insulin release and that there was no statistical interaction ($p = 0.801$) between these two parameters. The post hoc test results (Fisher's LSD) showed that insulin secretion was not statistically different in either cell type in the absence of glucose. However, both in presence of 5 and

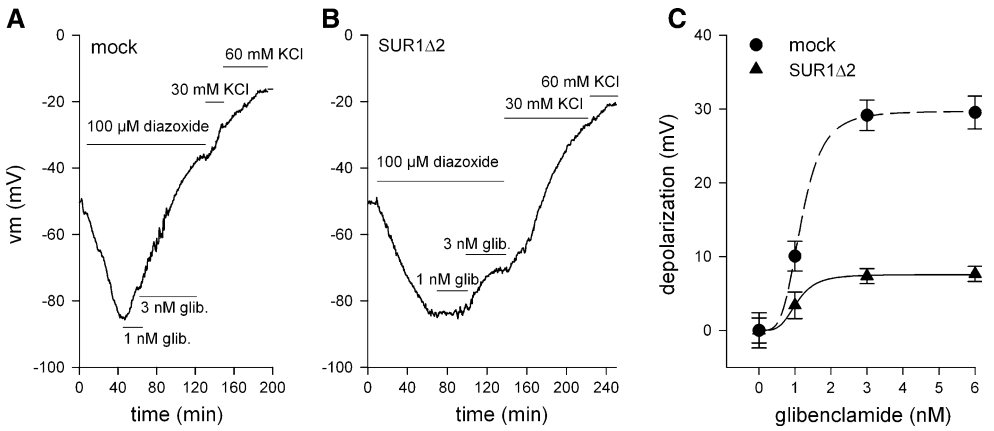

Fig. 8 SUR1Δ2 functionally displaces the sulfonylurea receptor action of SUR1. Effects of SUR1Δ2 transfection of RINm5F insulinoma cells on glibenclamide-induced depolarization. Using DIBAC4(3), a membrane potential-sensitive dye, membrane potentials were derived from cellular fluorescence. At steady state after dye uptake, cells were hyperpolarized with 100 μM diazoxide and subsequently treated with 1, 3 or 6 nM glibenclamide (glib). Representative time courses of membrane potentials of (**a**) mock- and (**b**) SUR1Δ2-transfected cells in response to 1 and 3 nM glibenclamide and to 30 as well as 60 mM KCl are shown. **c** Hill-type concentration response curves were fitted to mean glibenclamide-induced depolarizations ± SEM from $n = 30$ regions of interest (ROIs: usually single insulinoma cell clusters) of both mock- (*filled circles*) and SUR1Δ2-transfected cells (*triangles*). Non-linear regression curves are represented as a *dashed line* for mock- (EC50 = 1.15 nM, efficacy = 29.5 mV) and a *solid line* for SUR1Δ2-transfected cells (EC50 = 1.08 nM, efficacy = 7.7 mV)

10 mM glucose, mock-transfected cells released significantly more insulin than SUR1Δ2-transfected cells (Fig. 9e). In contrast to mock-transfected cells, there was only a very weak and statistically non-significant increase in insulin release with increasing glucose concentrations in SUR1Δ2 cells.

Discussion

In this work, we describe the discovery and functional characterization of a novel, truncated single-transmembrane peptide coded by an alternatively spliced human sulfonylurea receptor1 mRNA, termed SUR1Δ2, that is present in human pancreas, heart and other tissues together with SUR1. It has two remarkable properties: first, it functionally displaces high-affinity sulfonylurea receptor activity, and second, it has prodiabetic properties when expressed in insulinoma cells that lack endogenous SUR1Δ2. These findings could not only have high clinical relevance, but may also provide additional knowledge on the location and mode of molecular interaction between the regulatory sulfonylurea receptors and the pore-forming units of K_{ATP}-channel complexes.

SUR1Δ2 mRNA is present in human heart, pancreas and further tissues

Both a transcript scanning RT-PCR approach and 5′-RACE-PCR with cDNA prepared from human heart revealed the predominant presence of a SUR1 mRNA lacking exon 2, SUR1Δ2, which constitutes about 85% of all SUR1 transcripts. Such an almost exclusive SUR1Δ2 expression was found not only in heart, skeletal muscle, kidney and uterus, but also in testis. In tissues of the central nervous system the splice variant constituted between 60 and 80%. In pancreas, the relative abundance was lower than 50%. For the latter tissue, both SUR transcripts originated from islet cells, but not from exocrine cells, because the human SUR1 promoter contains binding motifs for the beta-cell-specific transcription factors Pdx-1 and IB1 [29]. The functional and clinical consequences of the presence of SUR1Δ2 in human heart and pancreatic beta-cells will be discussed below.

The tissue pattern correlated well with the tissue abundance profile of expressed sequence tags (ESTs) containing SUR1 sequences as published in the NCBI transcriptome database (UniGene accession number: Hs.54470). However, the Unigene database does not suggest expression of SUR1 in prostate, testis or uterus, while indicating very low SUR1 expression in lung and placenta. Nevertheless, the literature supports the validity of our results: The abundance of K_{ATP} subunits in human myometrium has been studied by quantitative RT-PCR and has indeed revealed a low, but unequivocal presence of SUR1 [30]. Furthermore, the presence of SUR1 mRNA has been confirmed independently in human transurethral resections of the prostate [31] and testis (spermatogenic cells) [32], while SUR1 has been reported to be absent in lung alveolar epithelial cells [33].

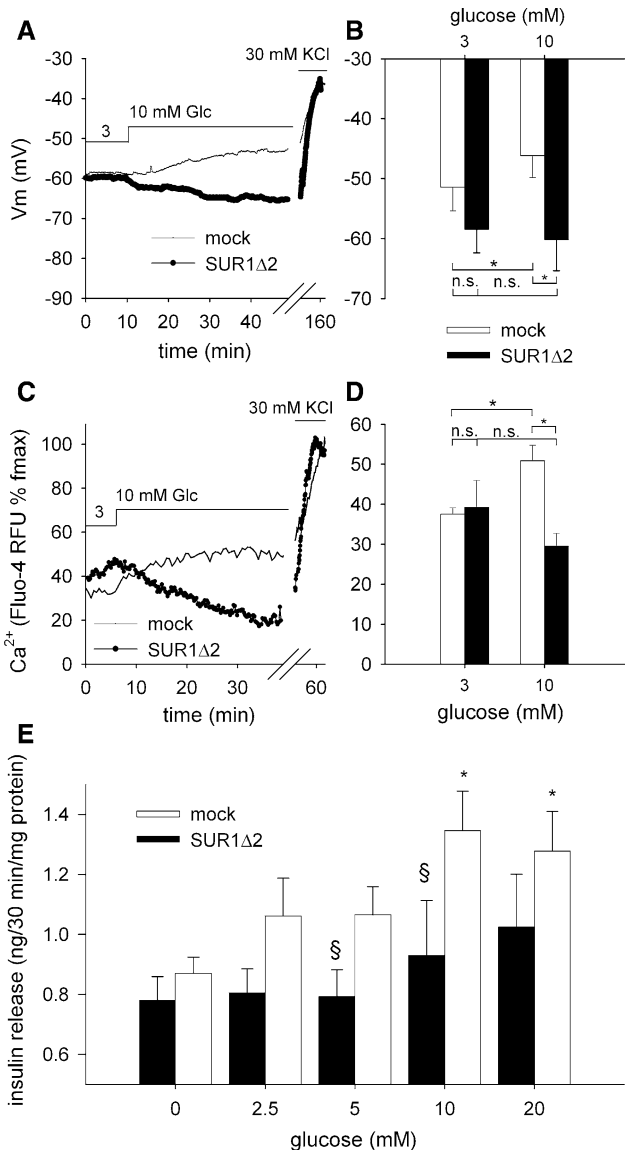

Fig. 9 SUR1Δ2 behaves as a prodiabetic peptide. Effects of SUR1Δ2 transfection on glucose-induced depolarization, cytosolic Ca^{++} and insulin release in RINm5F insulinoma cells. Representative time courses of fluorescence-derived membrane potentials (**a**) and cytosolic Ca^{++} (**c**) in response to a glucose (Glc) shift from 3 to 10 mM and to the addition of 30 mM KCl are shown for mock-transfected (*line*) and for SUR1Δ2-transfected cells (*line and scatter*). Results of $n = 4$ independent experiments in each group for membrane potential (**b**) and calcium data (**d**) are expressed as means ± SEM, $^{*}p < 0.05$ (paired *t* test between 3 and 10 mM glucose, Student's *t* test between SUR1Δ2- and mock-transfected groups). **e** Effect of SUR1Δ2 transfection on insulin release of RINm5F insulinoma cells. Cells were incubated for 30 min at 37°C with extracellular buffer and glucose at the indicated concentrations. Insulin content of the supernatant determined with sensitive RIA assay was normalized to the protein content of the cells in each well. A two-way ANOVA analysis was performed on the data ($n = 6$ independent experiments), showing that overall insulin secretion is highly significantly reduced ($p < 0.001$) as a result of SUR1Δ2 transfection. Statistically significant differences between individual groups in post hoc tests (Fisher's LSD) are shown: $^{\S}p < 0.05$ between SUR1Δ2- and mock-transfected groups, $^{*}p < 0.05$ compared to zero glucose

Skipping of exon 2 in humans is based on a weak first splice acceptor site

Splicing of pre-mRNA takes place in the spliceosome, a complex of small nuclear riboproteins (snRNPs) containing the U1,U2,U4, U5 and U6 subunits. U1 detects splice donor consensus sequences (C/AAG|gup$_u$agu) at the exon-intron boundary, while U2 binds to the intronic branch point (p$_y$np$_y$p$_y$p$_u$ap$_y$) with assistance of the auxiliary factors U2AF65 and U2AF35, which recognize the polypyrimidine tract at the end of the intron and the p$_y$ag|G sequence at the intron-exon boundary, respectively. Thus, the spliceosome complex A, consisting of U1, U2 and U2AF, determines the exact location of the intron to be spliced out [34] before cleavage by the activity of the remaining spliceosome subunits. If the splice acceptor site does not fully conform to its consensus sequence, U2 auxiliary factors do not bind well and may proceed to the next splice acceptor site. Thereby exon-inclusion becomes dependent on the presence of intronic or exonic splicing enhancers (ISE, ESE) and silencers (ISS, ESS), as well as the expression of further auxiliary regulatory snRNPs detecting them. This leads to skipping of one exon in a tissue-specific manner. As shown in this work, this was the case with human SUR1Δ2, because the first real splice acceptor site had a low probability as predicted by the neural network NETGENE. This seems to be based on an unusually high purine content of the polypyrimidine tract preceding the splice acceptor site at the intron 1/exon 2 border (ucu**ga** cu**g**ucucucccu**g**cagGAUGGGGAAGUCAGAGCUCC). In contrast, the purine content of the first splice acceptor site in rats was lower and consequently predicted to have a high splice probability. This explains the lack of the SUR1Δ2 splice variant in rats.

Since at least seven strong ESEs detected by the auxiliary factor ASF/SF2 were present at a relevant distance as predicted by ESE-finder http://rulai.cshl.edu/tools/ESE2/ [35], tissue-specific expression of ASF/SF2 negatively correlates with SUR1Δ2 abundance, as shown in Fig. 3e. The single nucleotide polymorphism Pro69Pro (SNP333, T > C) located in exon 2 [36] adds another ESE (CCC **C**GGG, Fig. 10a), which may be one reason explaining the observed inter-individual differences in SUR1Δ2.

SUR1Δ2 protein is a truncated transmembrane peptide (5.6 kD) with a single TM-helix

The SUR1Δ2 open reading frame (ORF) consisted of 153 nucleotides, and the corresponding protein was 50 amino acids long (5.6 kD): new Genebank accession no. HM635782.1. The entire peptide can best be described as a "cane" inserted into the membrane by its single transmembrane helix and protruding into the extracellular space

with its N-terminal "handle." An inverse peptide orientation could be ruled out because of N-glycosylation at the N-terminal side. SUR1Δ2 neither contained nucleotide-binding domains nor the sulfonylurea-binding subsites A and B (Fig. 2a): In SUR1, the Walker A and Walker B motifs of NBD1 are located in the cytosolic portion between TMD1 and TMD2, and that of NBD2 in the cytosolic loop C-terminal of TMD2, respectively [37]. The sulfonylurea-binding subsite A is located in TMD 2 of SUR1, whereby transmembrane segments 14 and 15 and parts of the adjacent cytosolic loops contribute [38] to it. The B-subsite involves parts of the cytosolic loop 3 (CL3), which connects TMD0 and 1 and extends to the N-terminus of Kir6.2 [39, 40].

SUR1Δ2 interacts with Kir6.2 and opens SUR1/Kir6.2 containing K_{ATP} channels

Using co-immunoprecipitation, we demonstrated that SUR1Δ2 physically associates with Kir6.2 pore-forming subunits of Kir6.2/SUR1 containing K_{ATP} channels. Our electrophysiological data suggest that the additional presence of the SUR1Δ2 peptide in these channels reduces their sensitivity for ATP inhibition. In contrast to SUR1, we found that SUR1Δ2 could be expressed on the plasma membrane by itself (in absence of Kir6.2) in COS-7 cells that endogenously lack all of these subunits. In addition, SUR1Δ2 could not form functional channels when co-expressed with Kir6.2 alone. This was most probably due to the fact that the ER-retention signal RKR present in Kir6.2 [41] could not be shielded by SUR1Δ2, and thus both remained entrapped in the ER. This is in agreement with our finding that surface expression of SUR1Δ2 was blunted in the presence of Kir6.2 (without SUR1). In triple-transfected cells a fraction of SUR1Δ2 (about 60%) associated with Kir6.2, and the other reached the plasma membrane independently of Kir6.2 expression. Nevertheless, the SUR1/SUR1Δ2/Kir6.2 complex trafficked to the plasma membrane when SUR1 was coexpressed. In additional support, elecrophysiological data showed that triple-transfected cells formed functional channels at the membrane, and the ATP sensitivity of these channels was decreased by a factor of about 6 compared to SUR1/Kir6.2 channels. This suggests the existence of hybrid SUR1Δ2/SUR1/Kir6.2 complexes with reduced ATP sensitivity, in which statistically about half of the four SUR1 subunits seemed to be replaced by SUR1Δ2, as shown in the SUR1/SUR1Δ2 surface expression assays.

Our results are in agreement with previous co-immunoprecipitation studies demonstrating a strong physical and functional association between the first transmembrane domain (TMD0) of SUR1 and Kir6.2 [42], where TMD0 alone also has an activating effect on a functional Kir6.2 variant lacking the RKR ER-retention signal. Thus, the results of the present work underline these findings and furthermore highlight the particular importance of the first transmembrane helix of TMD0, which contains the sulfonylurea receptor signature sequence GCFVDVLNVVPH VFLLFITFPILFIGWG, motif I-2 for binding to Kir6.2. This is the longest sequence of the 5-element N-terminal

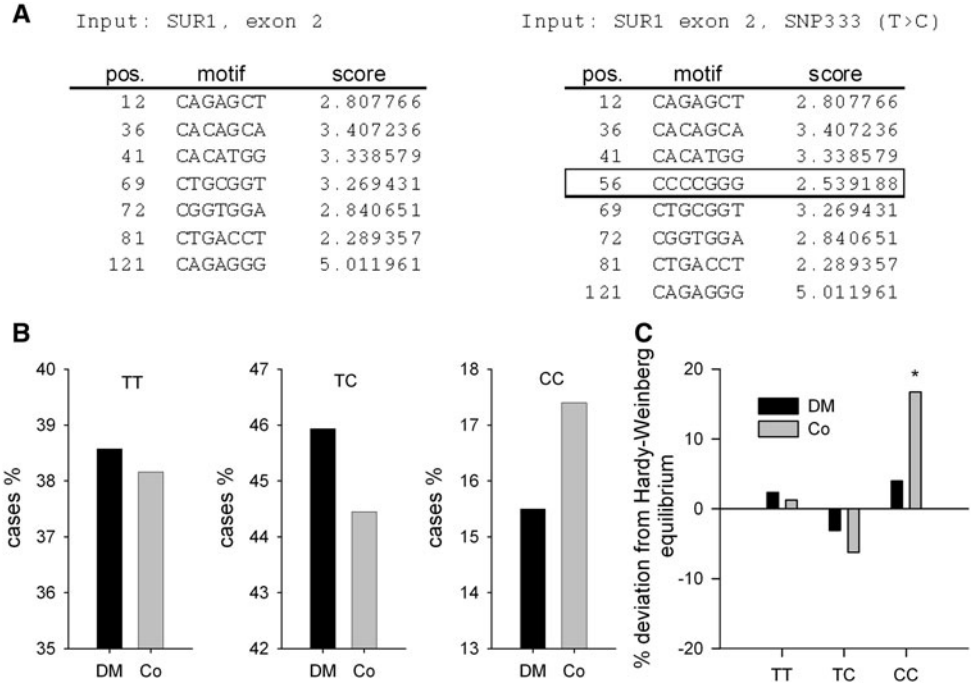

Fig. 10 The silent mutation Pro69Pro (SNP333) protects against diabetes. **a** Exonic splicing enhancer (ESE) sequences in exon 2 of SUR1 nucleotide detected by ASF/SF2 as predicted by the ESE-finder [35]. With a threshold value for strong ESEs of 2.0, seven ESEs were identified with a total score of 22.9. In exon 2 with SNP333 (T > C) an additional eighth ESE occurs (CCCCGGG), leading to a total score of 25.5. **b** Clinical data of 897 Japanese NIDDM patients (DM) and 891 healthy controls (Co) were taken from the literature [36] and further processed: The homozygotic SNP333 (CC) is more prevalent in healthy subjects than in diabetics. **c** Its prevalence significantly (*asterisks*) deviates from Hardy-Weinberg equilibrium in the healthy population

sulfonylurea receptor family fingerprint in TMD0 (accession: PR01092 in the SPRINT database, http://www.bioinf.manchester.ac.uk/dbbrowser/sprint/). It spans a small part of the N-terminus and the complete transmembrane helix 1 of SUR1 (Fig. 2c). The fact that motif I-2 is present and identical in SUR1, SUR1Δ2 and SUR2 [5], and that either of them is able to form complexes with Kir6.2 is indicative of the paramount role of the first transmembrane helix for the interaction between the pore-forming units and the regulatory SURs of K_{ATP} channels. In addition, motif I-2 is highly conserved between species, being equal at least in humans, rats, mice and black-bellied hamster.

Based on its functional properties, the novel splice variant SUR1Δ2 is suggested to represent a novel endogenous K_{ATP}-channel regulator with physiological and pathophysiological relevance, and importance for pharmacotherapy with sulfonylureas.

SUR1Δ2 functionally displaces high-affinity sulfonylurea action

A remarkable result of the present study is that transfection with SUR1Δ2 strongly reduced the ability of the sulfonylurea glibenclamide to depolarize RINm5F insulinoma cells. The pharmacological efficacy was reduced, but the potency was not altered, ruling out a direct displacement or competition at the high-affinity sulfonylurea-binding site. Rather, this finding could be explained by a functional displacement of SUR1 by SUR1Δ2 from its binding site on Kir6.2: SUR1Δ2 lacking both the sulfonylurea binding site(s) and the binding motifs for ATP/ADP of SUR1, which usually sensitize the K_{ATP} channel to ATP-mediated inhibition [43]. This was in accordance with the reduced ATP sensitivity of the SUR1Δ2/SUR1/Kir6.2 hybrid channel.

The observations may also enable us to understand the discrepancies in the ongoing sulfonylurea controversy [11, 44, 45]. Blockage of cardiac K_{ATP} channels impairs ischemic preconditioning and extends infarction areas [46]. Thus, cardiac K_{ATP} channels are considered to represent an endogenous cardioprotective mechanism usually attributed to SUR2A/Kir6.2-containing channels [47]. One of the major points of the controversy is whether human heart expresses high-affinity SUR1 that would lead to anti-cardioprotective effects of sulfonylurea drugs even at the low therapeutic concentrations used in therapy of type II diabetes. That this is not considered improbable is based on the fact that rat cardiac tissue displays high-affinity sulfonylurea binding [14] and human cardiac ventricular tissue contains SUR1 mRNA transcripts [13]. However, since we have demonstrated in our study that the predominant SUR1 transcript species in human heart is SUR1Δ2, any harmful effects of sulfonylurea on human heart might be negligible at therapeutic concentrations. We believe that our data represent a step forward in resolving the sulfonylurea controversy. Whether SUR1Δ2 interacts with SUR2/Kir6.2 containing K_{ATP} channels in cardiac tissue remains unclear. Since SUR2 shares the identical signature sequence with SUR1Δ2, an interaction with Kir6.2 and displacement of SUR2 is likely. However, the several fold higher abundance of SUR2 in heart compared to SUR1Δ2 possibly will limit the importance of such a mechanism.

SUR1Δ2 behaves as a prodiabetic peptide in insulinoma cells

The novel splice variant was expressed in human pancreas along with regularly spliced SUR1. In order to investigate the influence of SUR1Δ2 on the signaling of glucose-induced insulin secretion, RINm5F insulinoma cells were used, which were devoid of endogenous SUR1Δ2. However, regularly spliced SUR1 was expressed in these cells. Results showed that SUR1Δ2 not only fully blocks glucose-induced depolarization and cytosolic Ca^{++} release, but even caused a mild glucose-induced hyperpolarization and a decrease in cytosolic [Ca^{++}]. We conclude that the K_{ATP} channels remained activated despite increased glucose supply because their sensitivity to ATP was diminished by SUR1Δ2. The increased activity of electrogenic Na^+/K^+ and Ca^{++} ATPases at higher glucose and ATP levels led to hyperpolarization and a decreased cytosolic Ca^{++} level, as long as their effects were not counteracted by decreased potassium conductivity of K_{ATP} channels and increased L-Type calcium channel activity [48]. In further consequence, insulin secretion was reduced, as demonstrated, making SUR1Δ2 a prodiabetic peptide. Its presence in human pancreatic islet cells might thus shift the response characteristics and set point of beta-cells to higher glucose values. We suggest that in humans, genetic predisposition may lead to an increased SUR1Δ2 relative abundance, and hence higher resting glucose levels and a propensity to develop certain forms of type II diabetes associated with insufficient insulin release. These forms of diabetes may be additionally characterized by a restricted efficacy or even primary failure of sulfonylurea therapy in C-peptide-positive patients, which is not an uncommon clinical observation [49].

In contrast, factors that reduce SUR1Δ2 protected from diabetes mellitus: according to NCBI Entrez SNP database (http://www.ncbi.nlm.nih.gov/SNP), the SNP mentioned above (Pro69Pro, T > C, accession no.: rs1048099) is rather frequent (46% of all alleles in Caucasians). It generates an additional ESE detected by ASF/SF2 (Fig. 10a) that promotes inclusion of exon 2 (less SUR1Δ2) by a factor of 1.11 as calculated from the scores of ESE predictions. This SNP indeed confers a slight resistance to

diabetes, since according to a Japanese study [36] the homozygotic SNP (CC) is more prevalent in healthy controls (17.4%) than in NIDDM patients (15.4%, Fig. 10b). In addition, the prevalence of CC significantly deviates from Hardy-Weinberg equilibrium by an excess of 16.7% in healthy subjects, but not in diabetics (Fig. 10c), suggesting that it supports survival in the general population.

Acknowledgments Both Michael Stolzlechner and Albin Sorgner received a research grant from the Austrian Ministry of Science.

References

1. Noma A (1983) ATP-regulated K+ channels in cardiac muscle. Nature 305:147–148
2. Venkatesh N, Lamp ST, Weiss JN (1991) Sulfonylureas, ATP-sensitive K+ channels, and cellular K+ loss during hypoxia, ischemia, and metabolic inhibition in mammalian ventricle. Circ Res 69(3):623–637
3. Rorsman P (1997) The pancreatic beta-cell as a fuel sensor: an electrophysiologist's viewpoint. Diabetologia 40(5):487–495
4. Seino S, Miki T (2003) Physiological and pathophysiological roles of ATP-sensitive K+ channels. Prog Biophys Mol Biol 81(2):133–176
5. Babenko AP, Aguilar Bryan L, Bryan J (1998) A view of sur/KIR6.X, KATP channels. Annu Rev Physiol 60:667–687
6. Bryan J, Munoz A, Zhang X, Dufer M, Drews G, Krippeit-Drews P, Aguilar-Bryan L (2007) ABCC8 and ABCC9: ABC transporters that regulate K+ channels. Pflugers Arch 453(5):703–718
7. Chutkow WA, Simon MC, Le Beau MM, Burant CF (1996) Cloning, tissue expression, and chromosomal localization of SUR2, the putative drug-binding subunit of cardiac, skeletal muscle, and vascular KATP channels. Diabetes 45(10):1439–1445
8. Chutkow WA, Makielski JC, Nelson DJ, Burant CF, Fan Z (1999) Alternative splicing of sur2 exon 17 regulates nucleotide sensitivity of the ATP-sensitive potassium channel. J Biol Chem 274(19):13656–13665
9. Gros L, Trapp S, Dabrowski M, Ashcroft FM, Bataille D, Blache P (2002) Characterization of two novel forms of the rat sulphonylurea receptor SUR1A2 and SUR1BDelta31. Br J Pharmacol 137(1):98–106
10. Hambrock A, Preisig-Muller R, Russ U, Piehl A, Hanley PJ, Ray J, Daut J, Quast U, Derst C (2002) Four novel splice variants of sulfonylurea receptor 1. Am J Physiol Cell Physiol 283(2):C587–C598
11. Brady PA, Terzic A (1998) The sulfonylurea controversy: more questions from the heart. J Am Coll Cardiol 31(5):950–956
12. Ashfield R, Gribble FM, Ashcroft SJ, Ashcroft FM (1999) Identification of the high-affinity tolbutamide site on the SUR1 subunit of the K(ATP) channel. Diabetes 48(6):1341–1347
13. Elrod JW, Harrell M, Flagg TP, Gundewar S, Magnuson MA, Nichols CG, Coetzee WA, Lefer DJ (2008) Role of sulfonylurea receptor type 1 subunits of ATP-sensitive potassium channels in myocardial ischemia/reperfusion injury. Circulation 117(11):1405–1413
14. Gopalakrishnan M, Johnson DE, Janis RA, Triggle DJ (1991) Characterization of binding of the ATP-sensitive potassium channel ligand, [3H]glyburide, to neuronal and muscle preparations. J Pharmacol Exp Ther 257(3):1162–1171
15. Hussain K, Cosgrove KE (2005) From congenital hyperinsulinism to diabetes mellitus: the role of pancreatic beta-cell KATP channels. Pediatr Diabetes 6(2):103–113
16. Huopio H, Reimann F, Ashfield R, Komulainen J, Lenko HL, Rahier J, Vauhkonen I, Kere J, Laakso M, Ashcroft F, Otonkoski T (2000) Dominantly inherited hyperinsulinism caused by a mutation in the sulfonylurea receptor type 1. J Clin Invest 106(7):897–906
17. Flanagan SE, Clauin S, Bellanne-Chantelot C, de Lonlay P, Harries LW, Gloyn AL, Ellard S (2009) Update of mutations in the genes encoding the pancreatic beta-cell K(ATP) channel subunits Kir6.2 (KCNJ11) and sulfonylurea receptor 1 (ABCC8) in diabetes mellitus and hyperinsulinism. Hum Mutat 30(2):170–180
18. Hamill OP, Marty A, Neher E, Sakmann B, Sigworth FJ (1981) Improved patch-clamp techniques for high-resolution current recording from cells and cell-free membrane patches. Pflugers Arch 391(2):85–100
19. Klapperstuck T, Glanz D, Klapperstuck M, Wohlrab J (2009) Methodological aspects of measuring absolute values of membrane potential in human cells by flow cytometry. Cytometry A 75(7):593–608
20. Mittman S, Guo J, Agnew WS (1999) Structure and alternative splicing of the gene encoding alpha1G, a human brain T calcium channel alpha1 subunit. Neurosci Lett 274(3):143–146
21. Malboeuf CM, Isaacs SJ, Tran NH, Kim B (2001) Thermal effects on reverse transcription: improvement of accuracy and processivity in cDNA synthesis. Biotechniques 30(5):1074–1078 1080, 1082, passim
22. Jones DT (1999) Protein secondary structure prediction based on position-specific scoring matrices. J Mol Biol 292(2):195–202
23. Wu C, Orozco C, Boyer J, Leglise M, Goodale J, Batalov S, Hodge CL, Haase J, Janes J, Huss JW 3rd, Su AI (2009) BioGPS: an extensible and customizable portal for querying and organizing gene annotation resources. Genome Biol 10(11):R130
24. Brunak S, Engelbrecht J, Knudsen S (1991) Prediction of human mRNA donor and acceptor sites from the DNA sequence. J Mol Biol 220(1):49–65
25. Hough E, Beech DJ, Sivaprasadarao A (2000) Identification of molecular regions responsible for the membrane trafficking of Kir6.2. Pflugers Arch 440(3):481–487
26. Gribble FM, Ashfield R, Ammala C, Ashcroft FM (1997) Properties of cloned ATP-sensitive K+ currents expressed in *Xenopus* oocytes. J Physiol 498(Pt 1):87–98
27. Li L, Rojas A, Wu J, Jiang C (2004) Disruption of glucose sensing and insulin secretion by ribozyme Kir6.2-gene targeting in insulin-secreting cells. Endocrinology 145(9):4408–4414
28. Hussain M, Wareham AC (1994) Rundown and reactivation of ATP-sensitive potassium channels (KATP) in mouse skeletal muscle. J Membr Biol 141(3):257–265
29. Ashfield R, Ashcroft SJ (1998) Cloning of the promoters for the beta-cell ATP-sensitive K-channel subunits Kir6.2 and SUR1. Diabetes 47(8):1274–1280
30. Curley M, Cairns MT, Friel AM, McMeel OM, Morrison JJ, Smith TJ (2002) Expression of mRNA transcripts for ATP-sensitive potassium channels in human myometrium. Mol Hum Reprod 8(10):941–945
31. Haynes JM, Cook AL (2006) Protein kinase G-induced activation of K(ATP) channels reduces contractility of human prostate tissue. Prostate 66(4):377–385
32. Acevedo JJ, Mendoza-Lujambio I, de la Vega-Beltran JL, Trevino CL, Felix R, Darszon A (2006) KATP channels in mouse spermatogenic cells and sperm, and their role in capacitation. Dev Biol 289(2):395–405
33. Bardou O, Trinh NT, Brochiero E (2009) Molecular diversity and function of K+ channels in airway and alveolar epithelial cells. Am J Physiol Lung Cell Mol Physiol 296(2):145–155
34. Matlin AJ, Clark F, Smith CW (2005) Understanding alternative splicing: towards a cellular code. Nat Rev Mol Cell Biol 6(5):386–398

35. Cartegni L, Wang J, Zhu Z, Zhang MQ, Krainer AR (2003) ESE finder: a web resource to identify exonic splicing enhancers. Nucleic Acids Res 31(13):3568–3571
36. Sakamoto Y, Inoue H, Keshavarz P, Miyawaki K, Yamaguchi Y, Moritani M, Kunika K, Nakamura N, Yoshikawa T, Yasui N, Shiota H, Tanahashi T, Itakura M (2007) SNPs in the KCNJ11-ABCC8 gene locus are associated with type 2 diabetes and blood pressure levels in the Japanese population. J Hum Genet 52(10):781–793
37. Aittoniemi J, Fotinou C, Craig TJ, de Wet H, Proks P, Ashcroft FM (2009) Review. SUR1: a unique ATP-binding cassette protein that functions as an ion channel regulator. Philos Trans R Soc Lond B Biol Sci 364(1514):257–267
38. Winkler M, Stephan D, Bieger S, Kuhner P, Wolff F, Quast U (2007) Testing the bipartite model of the sulfonylurea receptor binding site: binding of A-, B-, and A + B-site ligands. J Pharmacol Exp Ther 322(2):701–708
39. Mikhailov MV, Mikhailova EA, Ashcroft SJ (2001) Molecular structure of the glibenclamide binding site of the beta-cell K(ATP) channel. FEBS Lett 499(1–2):154–160
40. Vila-Carriles WH, Zhao G, Bryan J (2007) Defining a binding pocket for sulfonylureas in ATP-sensitive potassium channels. Faseb J 21(1):18–25
41. Zerangue N, Schwappach B, Jan YN, Jan LY (1999) A new ER trafficking signal regulates the subunit stoichiometry of plasma membrane K(ATP) channels. Neuron 22(3):537–548. doi: S0896-6273(00)80708-4[pii]
42. Chan KW, Zhang H, Logothetis DE (2003) N-terminal transmembrane domain of the SUR controls trafficking and gating of Kir6 channel subunits. EMBO J 22(15):3833–3843
43. Shyng S, Ferrigni T, Nichols CG (1997) Regulation of KATP channel activity by diazoxide and MgADP. Distinct functions of the two nucleotide binding folds of the sulfonylurea receptor. J Gen Physiol 110(6):643–654
44. Lepor NE (2004) Diabetes mellitus. The sulfonylurea controversy: friend or foe? Rev Cardiovasc Med 5(2):134–135
45. Brady PA, Jovanovic A (2003) The sulfonylurea controversy: much ado about nothing or cause for concern? J Am Coll Cardiol 42(6):1022–1025
46. Suzuki M, Sasaki N, Miki T, Sakamoto N, Ohmoto-Sekine Y, Tamagawa M, Seino S, Marban E, Nakaya H (2002) Role of sarcolemmal K(ATP) channels in cardioprotection against ischemia/reperfusion injury in mice. J Clin Invest 109(4):509–516
47. Jovanovic A, Jovanovic S, Lorenz E, Terzic A (1998) Recombinant cardiac ATP-sensitive K+ channel subunits confer resistance to chemical hypoxia-reoxygenation injury [see comments]. Circulation 98(15):1548–1555
48. Dufer M, Haspel D, Krippeit-Drews P, Aguilar-Bryan L, Bryan J, Drews G (2009) Activation of the Na+/K+ -ATPase by insulin and glucose as a putative negative feedback mechanism in pancreatic beta-cells. Pflugers Arch 457(6):1351–1360
49. Bell DS, Mayo MS (1998) Improved glycemic control with use of oral hypoglycemic therapy with or without insulin. Endocr Pract 4(2):82–85